nks

Nordisk kernesikkerhedsforskning
Norrænar kjarnöryggisrannsóknir
Pohjoismainen ydinturvallisuustutkimus
Nordisk kjernesikkerhetsforskning
Nordisk kärnsäkerhetsforskning
Nordic nuclear safety research

NKS-55
ISBN 87-7893-109-6

Measurements of plume geometry and argon-41 radiation field at the BR1 reactor in Mol, Belgium

Martin Drews[1)], Helle Karina Aage[2)], Kim Bargholz[3)]
Hans Jørgensen[1)], Uffe Korsbech[2)], Bent Lauritzen[1)]
Torben Mikkelsen[1)], Carlos Rojas-Palma[4)] and Raf Van Ammel[4)]

[1)] Risø National Laboratory, Denmark
[2)] Technical University of Denmark
[3)] Danish Emergency Management Agency
[4)] Belgian Nuclear Research Center (SCK•CEN), Belgium

February 2002

Abstract

An atmospheric dispersion experiment was conducted using a visible tracer along with the routine releases of ^{41}Ar from the BR1 air-cooled research reactor in Mol. In the experiment, simultaneous measurements of the radiation field from the ^{41}Ar decay, the meteorology, the ^{41}Ar source term and plume geometry were performed. The visible tracer was injected into the reactor emission stack, and the plume cross section determined by Lidar scanning of the released aerosols. The data collected in the exercise provide a valuable resource for atmospheric dispersion and dose rate modeling.

Key words

Aerosols; Argon 41; BR-1 Reactor; Gamma Detection; Optical Radar; Plumes; Tracer Techniques.

NKS-55
ISBN 87-7893-109-6

Pitney Bowes Management Services Denmark A/S, 2002

The report can be obtained from
NKS Secretariat
P.O. Box 30
DK – 4000 Roskilde
Denmark

Phone +45 4677 4045
Fax +45 4677 4046
http://www.nks.org
e-mail nks@catscience.dk

NKS-55
ISBN 87-7893-109-6

Measurements of plume geometry and argon-41 radiation field at the BR1 reactor in Mol, Belgium

Project BOK-1.3

Martin Drews[1)], Helle Karina Aage[2)], Kim Bargholz[3)],
Hans Jørgensen[1)], Uffe Korsbech[2)], Bent Lauritzen[1)],
Torben Mikkelsen[1)], Carlos Rojas-Palma[4)] and Raf Van Ammel[4)]

1) Risø National Laboratory, DK-4000 Roskilde, Denmark

2) Technical University of Denmark, DK-2800 Kgs. Lyngby, Denmark

3) Danish Emergency Management Agency, DK-3460 Birkerød, Denmark

4) Belgian Nuclear Research Center (SCK•CEN), Boeretang 200, B-2400 Mol, Belgium

February 2002

Summary

An atmospheric dispersion experiment was carried out at the BR1 research reactor in Mol, Belgium, in October 2001 as collaboration between NKS and Belgian Nuclear Research Center (SCK•CEN), and with participation from SCK•CEN, Risø National Laboratory, the Technical University of Denmark, and the Danish Emergency Management Agency. In the experiment, artificial smoke was released from the 60-m reactor stack together with the routine emission of ^{41}Ar.

The main objective of the experiment was to gather information on the characteristics of a radioactive plume and to correlate these features with observed downwind spectral gamma-ray measurements. The resulting database of the environmental monitoring measurements may be used to validate atmospheric dispersion and dose rate models and to test data assimilation algorithms for short-range atmospheric dispersion.

The measurements consisted of four main components, carried out simultaneously: a) characterization of the ^{41}Ar source term originating from the emission stack of the BR1 research reactor, b) characterization of the meteorology during release c) characterization of the aerosol plume by Lidar scanning, and d) the monitoring of the gamma radiation field from the decay of ^{41}Ar.

The plume geometry was determined by the Lidar scanning technique: artificial smoke was injected into the reactor stack and the visible plume scanned by a pulsed laser beam. The wavelength of the laser beam is of the same order of magnitude as the mean aerodynamic diameter of the smoke particles, hence the crosswind shape and location of the plume may be determined through Mie scattering.

The radiation field was monitored by an array of eight NaI(Tl)-detectors properly calibrated and mounted in arrays perpendicular to the main advection direction. From the spectral information the ^{41}Ar primary photon fluence rate was derived. In addition, two high-resolution germanium detectors were set up to calibrate the NaI signals and to provide additional information on the variation of the radiation field along the plume centerline.

In the experiment, simultaneous plume geometry and radiation field data were recorded covering about 6 hours of reactor operation. These data have been arranged in a database, which may form a basis for further development of atmospheric dispersion model tools.

Table of contents

1 Introduction

Atmospheric dispersion and dose rate models form an integral part of nuclear emergency preparedness automated decision support systems. These models are intended to predict the atmospheric transport and deposition of radionuclides accidentally released from a nuclear installation and to assess the radiation exposure of the population. The models may broadly be divided into deterministic and probabilistic models. An example of a deterministic model is the Rimpuff mesoscale model for atmospheric dispersion and dose evaluation [1, 2, 3]. In this model the source term (i.e., the released activity) and meteorological data are assumed to be known quantities from which the plume geometry and the radiation field are determined.

In recent developments, however, probabilistic data assimilation models for atmospheric dispersion and dose rate evaluation are being devised that can incorporate data from automated or manual radiation monitoring networks. Such data can be used either to complement uncertain source term data or to substitute entirely this information in case of an unmonitored release from a nuclear installation. In the data assimilation models, prognoses of atmospheric dispersion are improved and updated taking into account both original source term data and incoming data from the radiation monitoring networks.

Generally both the deterministic and probabilistic models are based on simplified assumptions on the crosswind dispersion of radionuclides in a turbulent airflow, and it is thus important to test the validity of these models in realistic settings. Hence, a full-scale experiment of a radioactive release in which all relevant parameters are determined will contribute to the development of data assimilation models for nuclear emergency preparedness. Furthermore, data assimilation models require the uncertainties of the input parameters to be quantified. A full-scale experiment will allow for a determination of model uncertainties and parameter covariance.

In the ^{41}Ar experiment here reported, the aim was to perform a full characterization of the radioactive plume released from a nuclear reactor and to correlate these features with observed downwind spectral measurements. The experiment was carried out at the SCK•CEN BR1 research reactor in Mol, Belgium. ^{41}Ar originates from the activation of ^{40}Ar, which is a noble gas present in ambient air, and is routinely emitted from the reactor. Simultaneous measurements were performed of meteorology, the ^{41}Ar emission rate (the source term), the ^{41}Ar radiation field and the plume geometry, the latter being measured using Lidar scanning of a visible tracer injected into the reactor stack.

The objective of the experiment was to obtain data that can be used in testing and developing atmospheric dispersion model tools. A schematic illustration of the experiment objectives is shown below in Figure 1. Data obtained in the experiment serves to validate atmospheric dispersion and dose rate models, for which the source term and meteorological data are input parameters. However, the same data set can also be used in the testing and development of data assimilation models for source term estimation. Here the meteorology and radiation monitoring data are input parameters, and the aim is to assess the plume geometry and the release rate.

This report contains a complete description of the experimental setup (Section 2) as well as each of its components (Sections 3-7). Furthermore, a few examples of the acquired data are presented. A detailed analysis of the data will be referred to a future publication.

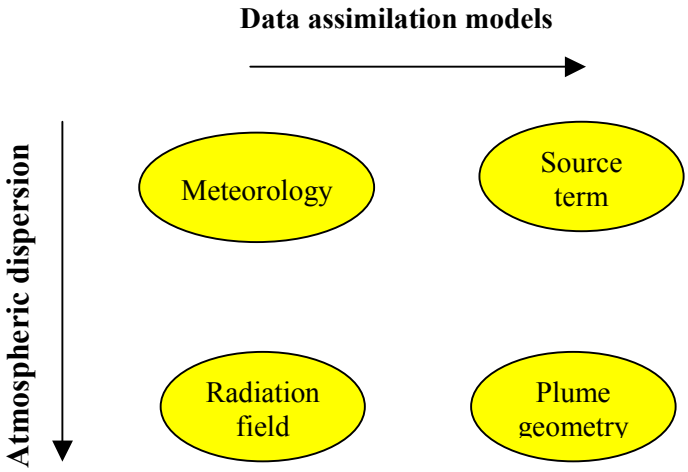

Figure 1. Components of the ^{41}Ar field experiment.

1.1 Experimental layout

The Belgian Nuclear Research Center (SCK•CEN) technical domain covers an area of approx. 1 km^2, with most of the premises comprising storage buildings, cf. Figure 2. The domain as well as the BR1 research reactor is situated in a rather level, forested area, intermittent with open grass fields. The vegetation mainly consists of coniferous trees. The predominant wind direction during the experiment was from the southwest (SW).

The BR1 is an air-cooled, graphite-moderated research reactor that can operate at a nominal 2 MW thermal effect. During the experiment, however, the reactor output was kept at 700 kW. At this effect atmospheric air is led through the reactor at the rate of 9.4 m^3 s^{-1} and is emitted from the 60-m stack, giving rise to a routine ^{41}Ar emission rate of approx. 1.5 x 10^{11} Bq h^{-1}. The actual emission rate is recorded by the permanent monitoring system mounted inside the ventilation shaft.

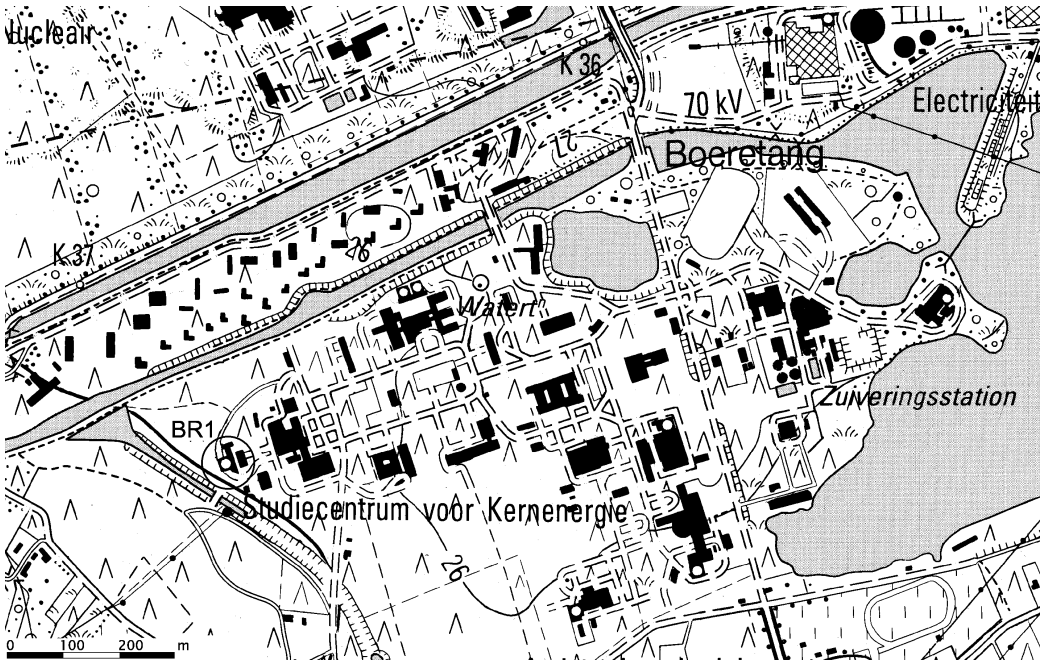

Figure 2. Overview of the SCK•CEN site at Mol, Belgium. The BR1 reactor stack is marked by a circle.

Meteorological observations of wind speed and wind direction, temperature gradients, and precipitation were performed with permanent instruments mounted on the SCK•CEN weather mast.

The radiation measurements took place both inside and outside the premises, at distances up to 1500 m downwind from the reactor stack. The radiation field was monitored by an array of eight NaI(Tl)-detectors properly calibrated and mounted in arrays perpendicular to the main advection direction. In addition, two high-resolution germanium detectors were set up to calibrate the NaI signals and to provide additional information on the variation of the radiation field along the plume centerline. The gamma detectors were mostly deployed along open stretches or along smaller roads in the area, for easy access and to avoid shielding from trees.

The plume geometry was determined by a Lidar scanning technique: a white aerosol tracer was injected into the reactor stack and the resulting plume, emitted from the top of the stack, was scanned by a pulsed laser beam. The Lidar scanning was performed using mobile Lidar scanning equipment (mounted on a bus) and placed either close to the reactor stack or further away, next to the gamma detectors.

The experiment was carried out over a period of five days, from Monday October 1st to Friday October 5th, 2001. The first two days were used for setting up and testing the equipment: smoke generator system, Lidar bus and gamma detectors, and for carrying out trial background measurements. Full-scale measurements were performed from Wednesday to Friday. Friday afternoon the gamma detectors were calibrated, cf. Table 1.

Table 1. Time schedule of experiment

Monday - Tuesday	Set-up of smoke generation system: Chemical mixing system, mounting injection hose inside reactor stack. Setup and testing of Lidar bus. Setup and testing of NaI and HPGe gamma detectors. Background measurements.
Wednesday - Thursday	Full-scale measurements of aerosol plume and ^{41}Ar radiation field.
Friday	Full-scale measurements continued. Calibration of gamma-detectors.

1.2 Detector identification

A collection of different detectors supplied by the participating organizations were used for the experiment. The detector identifiers are listed in Table 2.

Table 2. Definition of detector names

Detector	Description
DK-A, DK-B, DK-C, DK-D	NaI(Tl) detectors belonging to the Danish Emergency Management Agency (DEMA).
SCK-1, SCK-2, SCK-3, SCK-4	NaI(Tl) detectors belonging to the SCK•CEN.
DTU-HPGe	Germanium detector belonging to the Technical University of Denmark (DTU).
SCK-HPGe	Germanium detector belonging to the SCK•CEN.
Lidar bus	A mobile Lidar detection system built by the Wind Energy Department of the Risø National Laboratory.

2 Positions and time series

Actual measurements were carried out over a period of three days, from the morning of Wednesday, October 3rd, to Friday afternoon. The result was four series of measurements, covering a total of about 14 hours. The first series from Wednesday morning, however, was performed with only half the detectors in operation. The time series recorded with all equipment in place correspond to approximately 6 hours of continuous monitoring.

2.1 Experimental time synchronization

All experimental clocks were synchronized with the clock of the weather mast located inside the technical domain of the SCK•CEN. Apart from this synchronization the radiation measurements, the Lidar measurements, the source term measurements and the meteorological measurements were performed independently of each other. The recorded data was given time stamps for the onset of each measurement.

2.2 Detector positions

Figures 3-6 show the actual positions for all gamma detectors as well as the stack and the Lidar bus, and in Table 3 the UTM coordinates of the positions are listed. The scale of the maps is 1:10.000.

To determine the coordinates of the detectors and the Lidar bus, these were plotted on the map based on measured distances to specified fix-points. Subsequently, a UTM grid was copied onto each of the maps from a similar map of scale 1:25.000, and the positions were read off from the map. The absolute positions of all detectors and the Lidar bus have an estimated uncertainty of about 10 m, corresponding to a resolution of 1 mm on the maps. Comparing the distances between the detectors derived from the UTM coordinates and the recorded distances show that these coincide within the 10-m resolution.

Table 3. Detector positions in abbreviated 4-digit UTM coordinates. The UTM grid zone is 31U. To obtain the complete coordinates, add 06 to the east and 56 to the north coordinates, e.g. (4615, 7691) → (064615, 567691). The coordinates correspond to 10 m precision.

	Wed morning Oct 3rd		Wed afternoon Oct 3rd		Thursday Oct 4th		Friday Oct 5th	
Detector	**E**	**N**	**E**	**N**	**E**	**N**	**E**	**N**
DK-A	4615	7691	4637	7671	4585	7649	4577	7645
DK-B	4624	7695	4640	7662	4593	7654	4585	7649
DK-C	4607	7686	4635	7679	4579	7646	4569	7642
DK-D	4599	7682	4632	7687	4572	7643	4561	7638
SCK-1			4632	7686	4592	7679	4538	7651
SCK-2			4635	7679	4601	7683	4546	7655
SCK-3			4637	7670	4610	7687	4555	7660
SCK-4			4640	7662	4618	7692	4563	7664
DTU-HPGe	4625	7695	4582	7632	4589	7639		
SCK-HPGe			4583	7629	4579	7631	4558	7661
Lidar bus			4584	7624	4584	7624	4532	7648
BR1	4565	7621	4565	7621	4565	7621	4565	7621

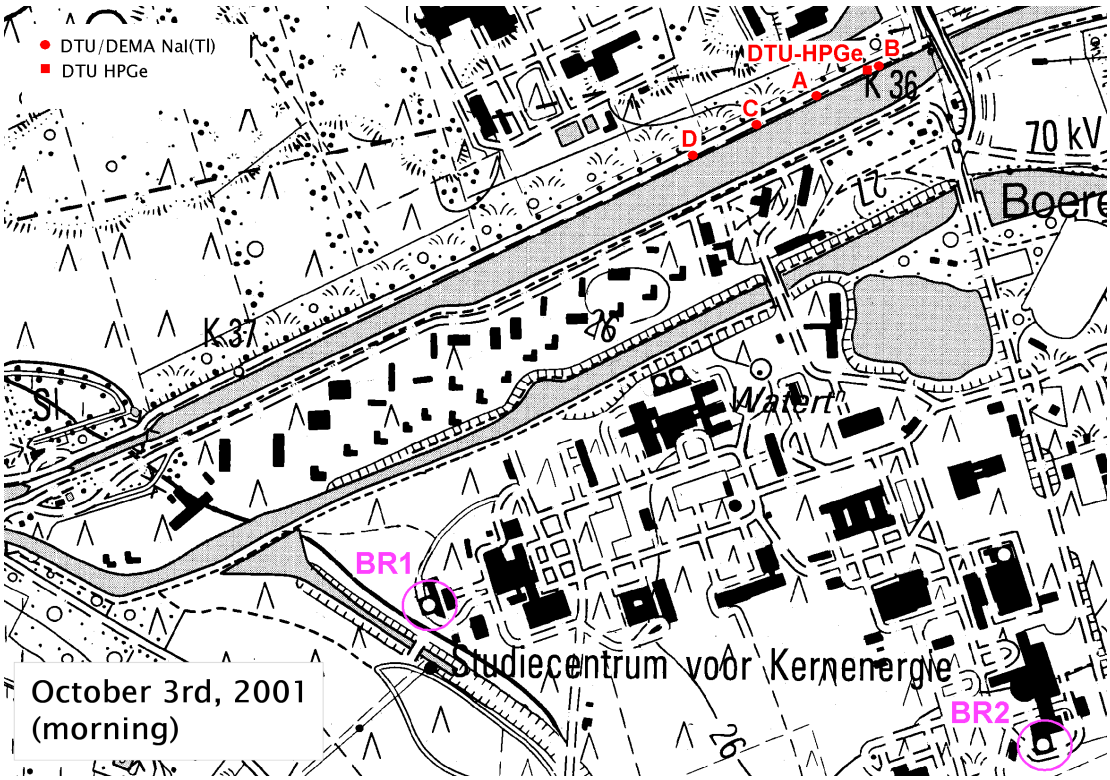

Figure 3. Experimental setup. The morning of October 3rd.

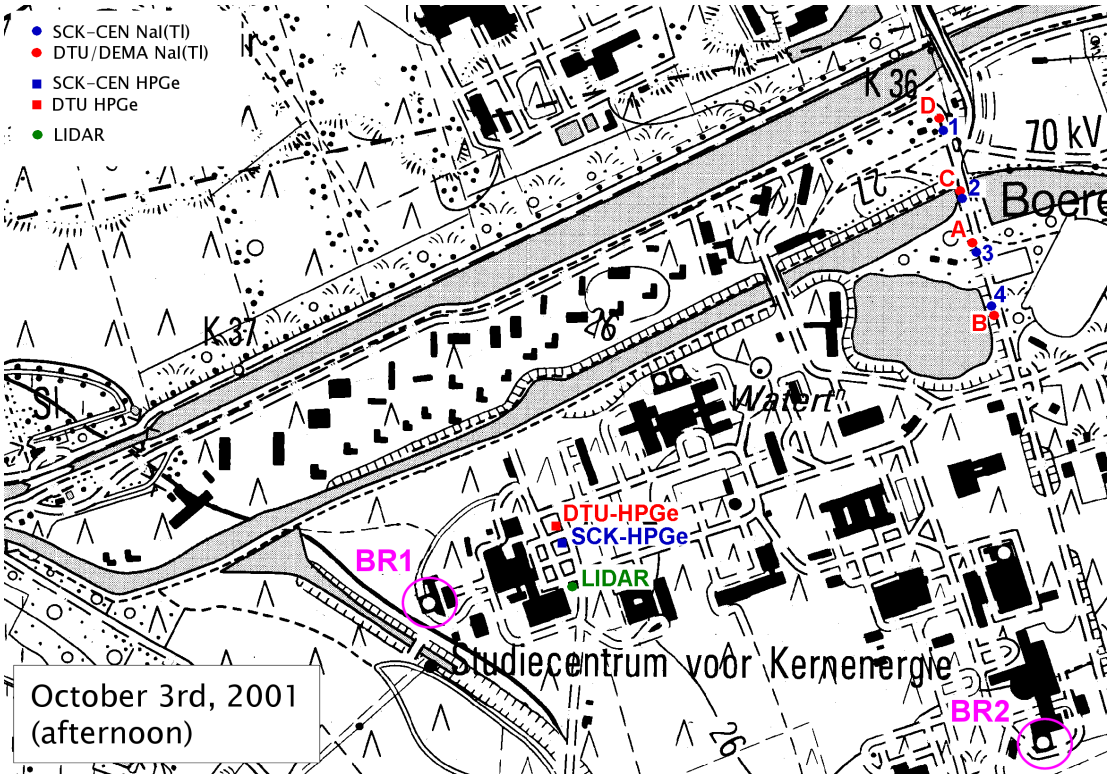

Figure 4. Experimental setup. The afternoon of October 3rd.

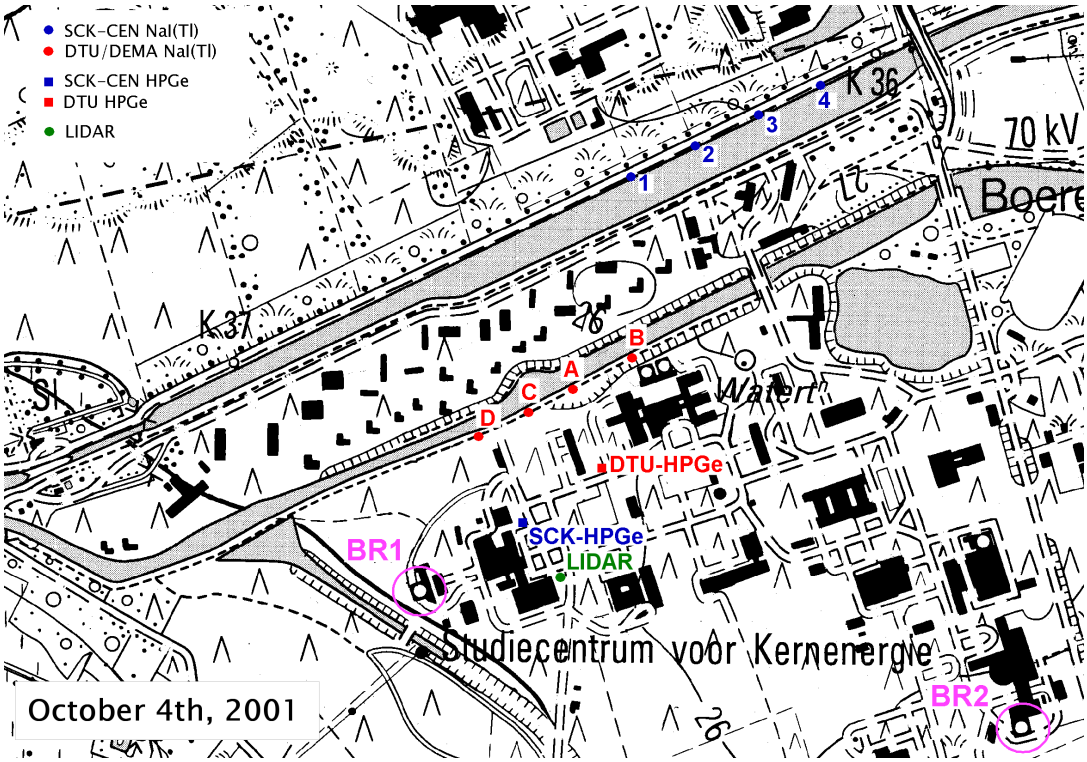

Figure 5. Experimental setup. October 4th.

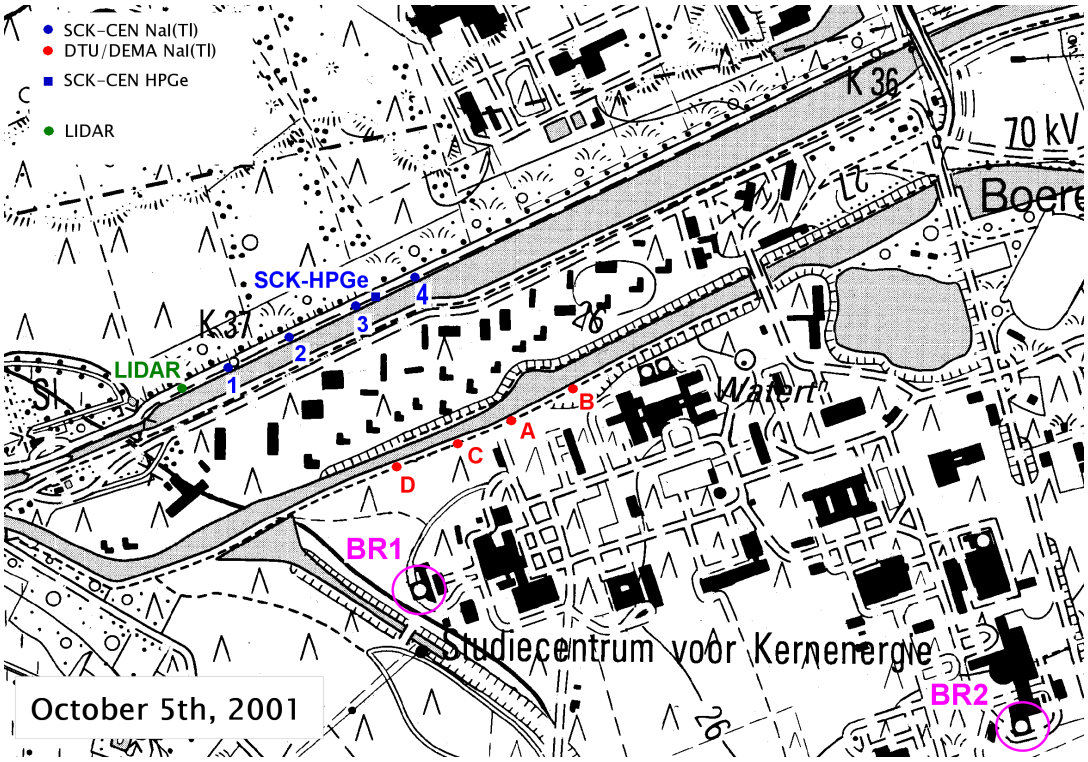

Figure 6. Experimental setup. October 5th.

2.2.1 NaI detector positions

Two different schemes were employed for the positioning of the NaI detectors as illustrated in Figure 7. In both cases the detectors were positioned approximately 100 m apart along a line roughly perpendicular to the plume centerline, the downwind distance from the reactor stack ranging from a few hundred meters and up to 1500 m. The aim was to cover the full width of the plume and to make the angle covered by the detectors wide enough also to accommodate minor shifts in the wind direction without moving the detectors. Fortunately, the wind direction generally proved sufficiently constant to allow the detectors once set up to remain in place. Only for Wednesday, October 3rd, they had to be moved, hence the two different time series recorded for this day.

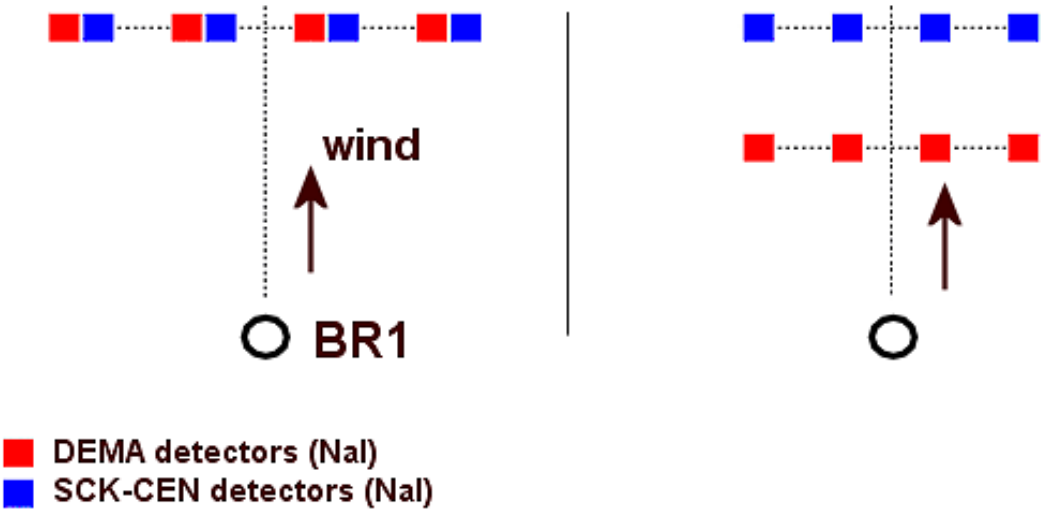

Figure 7. Sketch of the NaI detector setup. The detectors are set up along lines roughly perpendicular to the plume centerline.

The setup in the left part of Figure 7, where the detectors are placed pair wise, was employed for the measurements in the afternoon of October 3rd. This scheme allowed intercalibration of the DK and the SCK NaI detectors.

For the measurements of October 4th and October 5th, the NaI detectors were placed along two separate lines as shown in the right part of Figure 7. In this scheme both crosswind and downwind variations of the radiation field were measured.

In the morning of October 3rd only four detectors were available (cf. Figure 3). They were placed along a single straight line perpendicular to the plume centerline with a detector spacing of approximately 100 m.

2.2.2 Lidar bus and HPGe detector positions

The positions of the Lidar bus and HPGe detectors are shown in Figures 3-6. Ideally, the cross section plane of the Lidar scanning should include one of the lines of the NaI-detector array. Due to practical problems, however, on both Wednesday and Thursday the Lidar bus was placed closer to the reactor stack than the NaI-detectors. Only for the measurements Friday, the Lidar scanning was carried out along the line of one of the NaI-detector arrays (Figure 6).

The aim of the HPGe detectors was to provide supplementary high-resolution spectral information. Wednesday morning and Friday morning the available HPGe detector was placed next to one of the NaI detectors for calibration purposes, while for Wednesday afternoon and Thursday the HPGe detectors were placed close to the Lidar bus.

2.3 Recorded time series

The time series recorded by the individual detectors are pictured graphically in Figures 8-10. Small time intervals without data recording were typically due to the re-starting of the automatic data acquisition systems after completion of a period of measurements. Also, the NaI detector systems were periodically energy-calibrated as to avoid spectral drift.

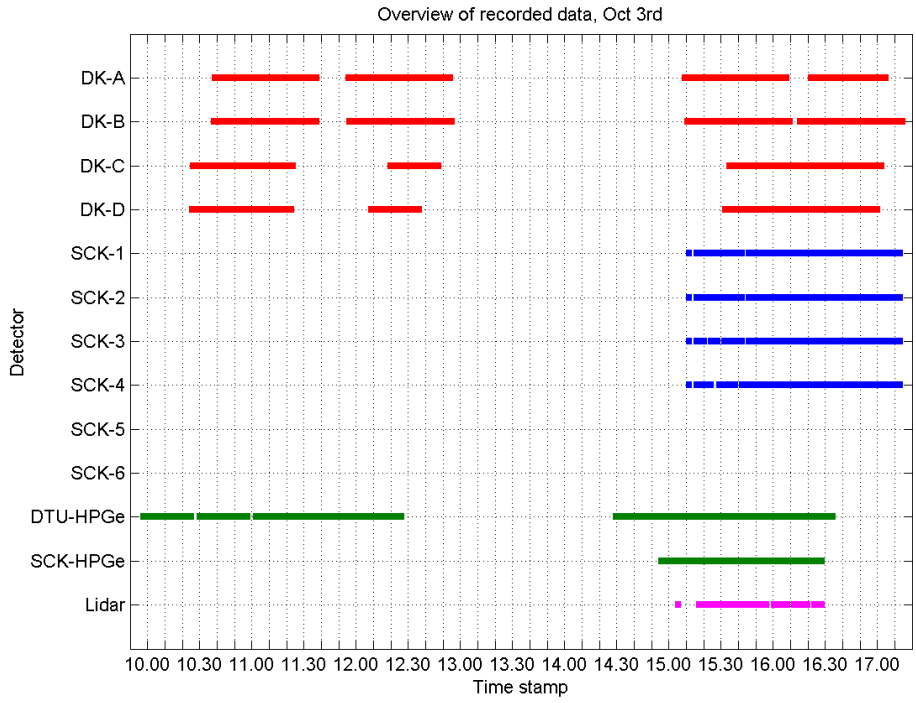

Figure 8. Time series acquired on Wednesday, October 3rd.

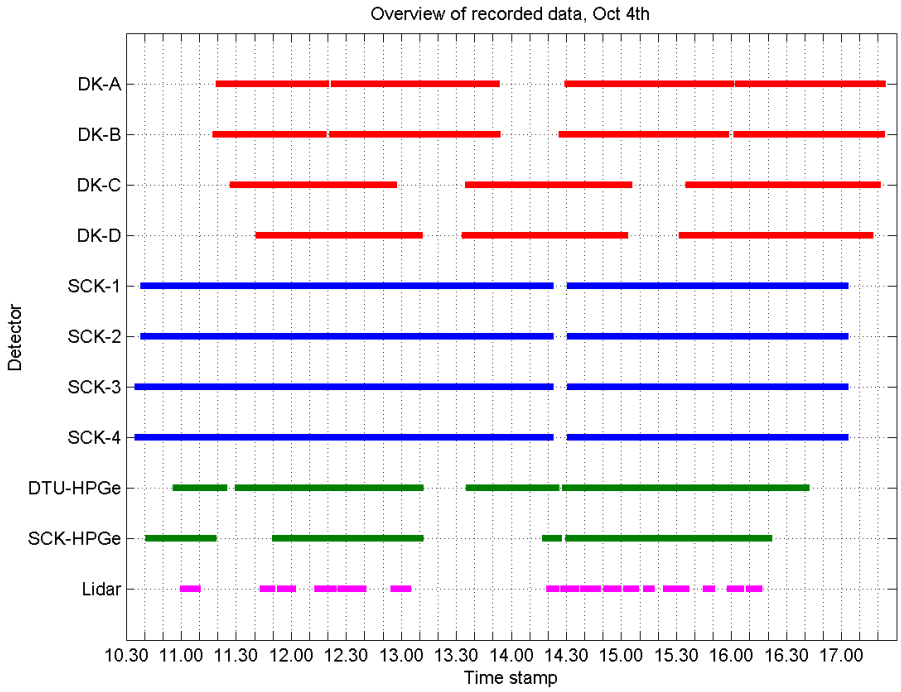

Figure 9. Time series acquired on Thursday, October 4th.

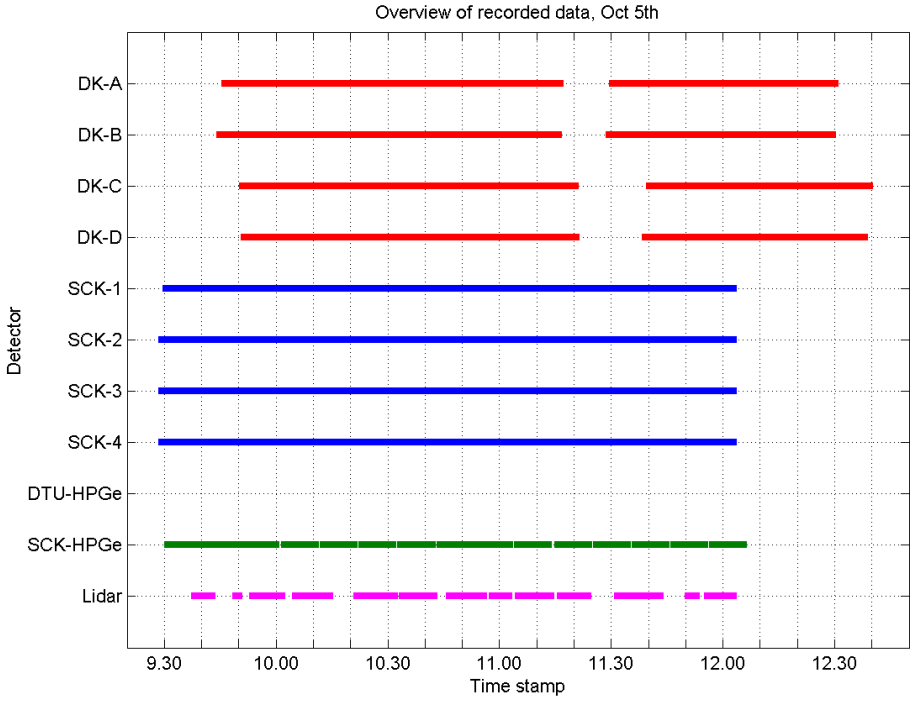

Figure 10. Time series acquired on Friday, October 5th.

3 Meteorology

During the experiment, the deployment and positioning of the gamma ray detectors and spectrometers were carefully planned using the readings from the SCK•CEN weather mast in addition to numerical weather prediction data provided by the Royal Belgian Meteorological Institute. Example data is shown in Figure 11, depicting the 6-h numerical weather prediction of surface winds for October 5th, 2001.

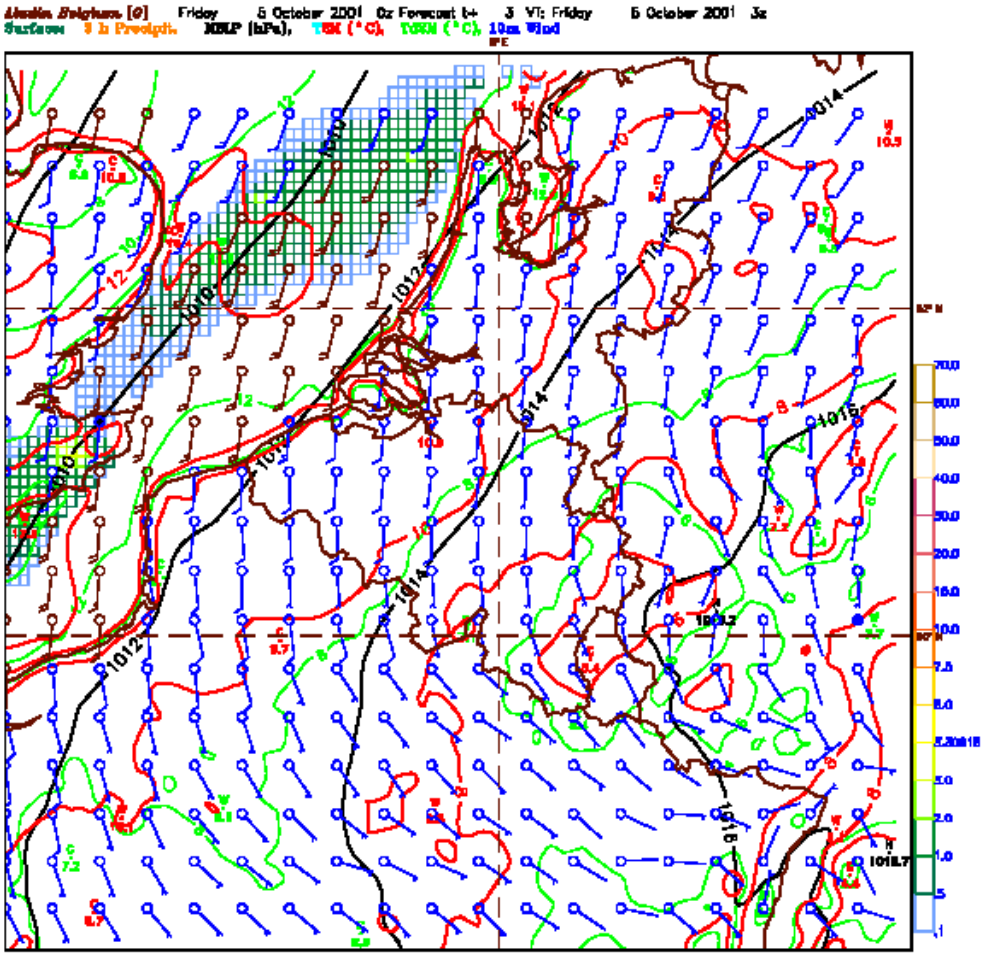

Figure 11. Wind surface predictions from the Royal Belgian Meteorological Institute.

The weather mast at the SCK•CEN collects data at the heights 8, 24, 48, 69, 78 and 114 m. The quantities measured are temperature, wind direction, wind speed, and precipitation intensity. In addition an environmental radiation monitor is located at the foot of the mast. The observations are logged, quality controlled and stored in a SQL database from which they are available to all applications and programs that require meteorological data, including local nuclear emergency response systems.

Figure 12. The SCK•CEN weather mast.

3.1 Meteorology and dispersion parameters

The local dispersion meteorology was extracted using direct measurements from weather mast located inside the SCK•CEN perimeters. The mast has several levels of instrumentation, but since the site is characterized by tall trees (~20 meter tall canopy), useful meteorology data were extracted solely from the level above the treetops. Only the following data was used from the weather mast: Wind speed measurements at 69 m and 78 m. Wind direction at 69 m. Temperature differences were estimated from thermometers at 48 m and 78 m height.

Based on these measurements, the scale micro-meteorological pre-processor of Astrup et al. [4] was used to extract dispersion scaling parameters, such as friction velocity, Monin-Obukhov stability length scale, and Pasquill-Gifford-Turner stability parameters. These data, suitable as input parameters for dispersion models, were calculated for 10 min averaging time intervals throughout the experiment periods.

4 Argon-41 source term

The amount of activity released during reactor operation (the source term) is determined from the airflow and the ^{41}Ar activity concentration in the stack. The flow rate during normal operation (700 kW) is 34,000 $m^3\ h^{-1}$. A plastic scintillator mounted with a photomultiplier is used to determine the activity concentration. The detector readings (cf. Figure 13) have been calibrated for ^{41}Ar, ^{133}Xe and ^{85}Kr, the calibration factors being

^{41}Ar: 20,000 Bq m^{-3} per channel

^{133}Xe: 45,500 Bq m^{-3} per channel

^{85}Kr: 27,000 Bq m^{-3} per channel

With a thermal power of 700 kW, the detector readings are approximately at 220 channels corresponding to a ^{41}Ar source term of about $1.50 \cdot 10^{11}$ Bq h^{-1}.

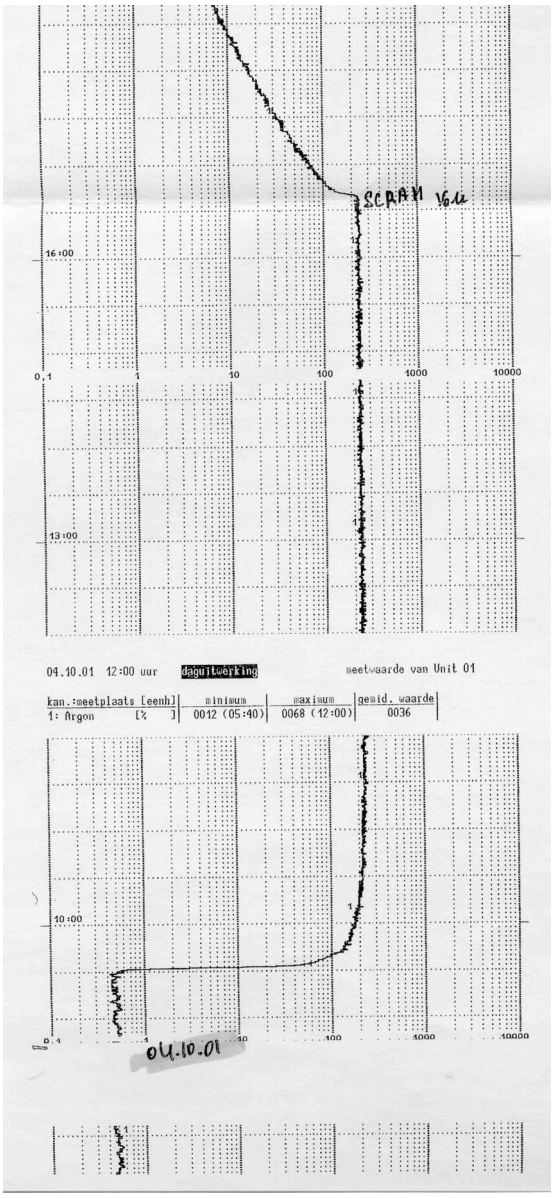

Figure 13. Monitoring data for the ^{41}Ar source term; printout from October 4th.

5 Radiation measurements

The radiation measurements were performed using two arrays of NaI(Tl) gamma detectors, provided by the Danish Emergency Management Agency (DEMA) and by SCK•CEN. Furthermore, two high precision germanium detectors (HPGe) provided by SCK•CEN and the Technical University of Denmark (DTU) were used for calibration and precision measurements.

5.1 NaI scintillators

The DEMA detector setup consisted of four thermally insulated 3" x 3" NaI(Tl) detectors of the same type as used by DEMA in permanent radiation monitoring networks. The detectors, labeled DK-A to DK-D, were each connected to a separate PC and could thus be set up independently of each other. For practical reasons, two of the PCs (DK-A and DK-B, respectively, DK-C and DK-D) were always placed together in order to be able to share a portable 220 V generator. Also, the length of the connecting cables was 50 m; hence the actual distance between the two detectors sharing a generator was limited to about 100 m. The DK-NaI detectors recorded a 512-channel spectrum every 30 seconds. Little or no spectrum drift was observed.

The SCK•CEN detector setup consisted of an array of four 2" x 2" NaI(Tl) crystals, labeled SCK-1 to SCK-4, each connected to a single-channel counter (Figure 14). Unlike the DK-NaI detectors, all the counters were interfaced through an analog-digital converter to a common PC for data acquisition and storage. A wide ^{41}Ar window was set for each of the SCK-NaI detectors, as the NaI crystals were not thermally insulated and therefore vulnerable to spectral drift.

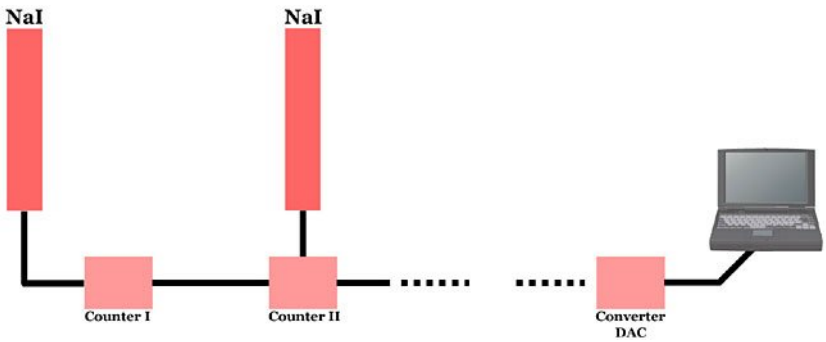

Figure 14. The SCK•CEN NaI detector array used in this experiment.

Figure 15. Setting up NaI detectors along the channel. Lidar scanning was performed the same place on Friday, October 5th.

5.1.1 DK-NaI detector calibration

The DK-NaI detectors were calibrated *on site* using a ^{60}Co point source of activity Q = 246.7 kBq produced by Amersham; the source activity was certified by the producer.

Two different calibration setups were employed. In the first setup, the four DK-NaI detectors were arranged in the corners of a 2 m x 2 m square with the ^{60}Co point source placed in the center of the square, cf. Figure 16. The detector orientations were equivalent to the orientation used in the field measurements, the crystal end of the detectors pointing upwards. The source was placed at approximately the same height above the ground as the center of the NaI crystals. In the second setup, the DK-NaI detectors were calibrated pair-wise. Two detectors were placed in horizontal position, "bottom-to-bottom", at a distance of 2 m with the calibration source in the center (Figure 17).

A summary of the calibration measurements is given in Table 4; here R is the distance from the cobalt source to the estimated center of radiation in the NaI crystals for 1.0-1.5 MeV photons. The primary photon fluence rate, φ, is calculated as

$$\varphi = Q \cdot \frac{y}{4\pi \cdot R^2} \cdot e^{-\mu_{air} \cdot R} \cdot e^{-\mu_{plastic} \cdot d},$$

where y is the γ-yield (99.98% and 99.90%, respectively, for the 1332.5 MeV and 1173.2 MeV photons from ^{60}Co), and μ_{air} and $\mu_{plastic}$ are the linear attenuation coefficients in air and in the plastic encasing of the cobalt source, respectively. The plastic encasing is rectangular, and in the first setup the effective thickness of the shielding, d, was about 0.3 mm. For setup 2 the value of d was 0.2 mm.

Figure 16. NaI detector calibration. The white barrels in the foreground contain the DK-NaI detectors (setup 1).

Figure 17. NaI detector calibration. Setup 2.

Table 4. Calibration setup.

Setup	Description	R (cm)	φ (m^{-2} s^{-1})	no. of meas.	Live time (s)
1	Square	141	9670	2	300
2	Bottom-to-bottom	100*	19400	2	180

* The actual distance varied by a few centimeters for each detector.

The detector efficiency, ε, is defined as

$$\varepsilon = r / \varphi,$$

where r is the net window count rate for the full energy peak, corrected for background. Figure 18 shows the ^{60}Co spectrum for detector DK-D in setup 1 as well as the background spectrum. The net window count rate of the 1332.5 keV peak was obtained by subtracting the background spectrum from the full window count rate. The window containing the 1173.2 keV peak, however, also contains a Compton background arising from primary photons of energy 1332.5 keV. Hence, to account for these Compton scattered photons, a linear background (indicated by a dashed line in the figure) was subtracted to obtain the net window count rate for 1173.2 keV window.

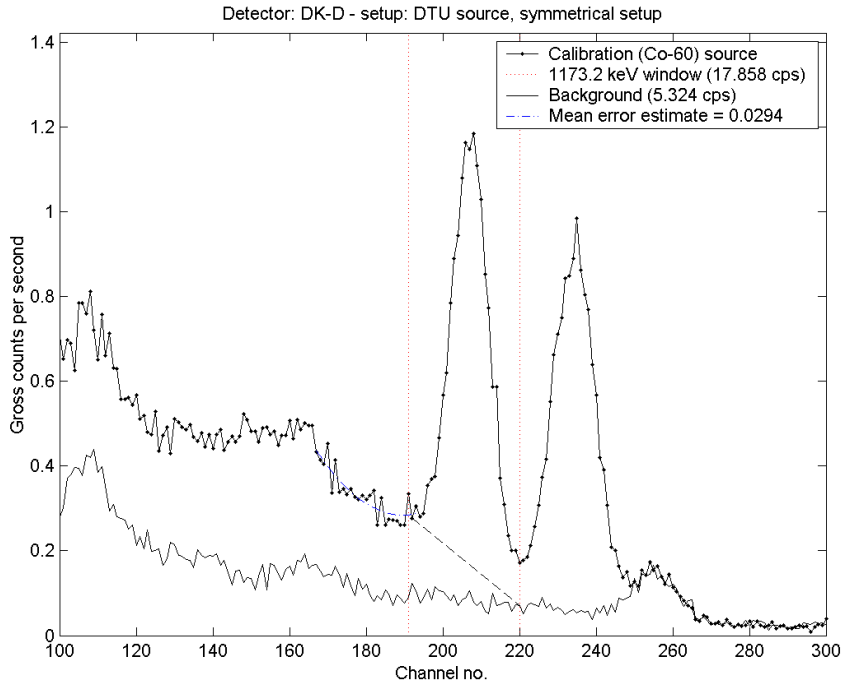

Figure 18. A trial ^{60}Co calibration spectrum.

The resulting detector efficiencies for ^{60}Co are shown in Tables 5-6 for setups 1 and 2, respectively. The detector efficiency for ^{41}Ar (E_γ = 1293.6 keV) was obtained by interpolation by assuming a simple linear energy dependency, cf. Figure 19.

The difference between the detector efficiencies found for setup 1 and 2 is due to the different orientations of the detectors (vertical vs. horizontal) in agreement with a previous study of the angular properties of the DK-NaI detector performed by the DTU.

Table 5. Calculated efficiencies for setup 1.

Detectors	$\langle r \rangle_{1173}$ (cps)	ε_{1173} (m^2)	$\langle r \rangle_{1332}$ (cps)	ε_{1332} (m^2)	ε_{1293} (m^2)
DK-A	17.7	0.00134	14.1	0.00127	0.00129
DK-B	17.4	0.00127	14.1	0.00126	0.00127
DK-C	17.1	0.00130	14.1	0.00125	0.00126
DK-D	17.9	0.00130	14.1	0.00125	0.00126

Table 6. Calculated efficiencies for setup 2.

Detectors	$\langle r \rangle_{1173}$ (cps)	ε_{1173} (m^2)	$\langle r \rangle_{1332}$ (cps)	ε_{1332} (m^2)	ε_{1293} (m^2)
DK-A	29.0	0.00113	23.2	0.00110	0.00111
DK-B	30.0	0.00119	23.6	0.00112	0.00114
DK-C	29.0	0.00119	22.8	0.00111	0.00113
DK-D	29.7	0.00117	23.6	0.00112	0.00114

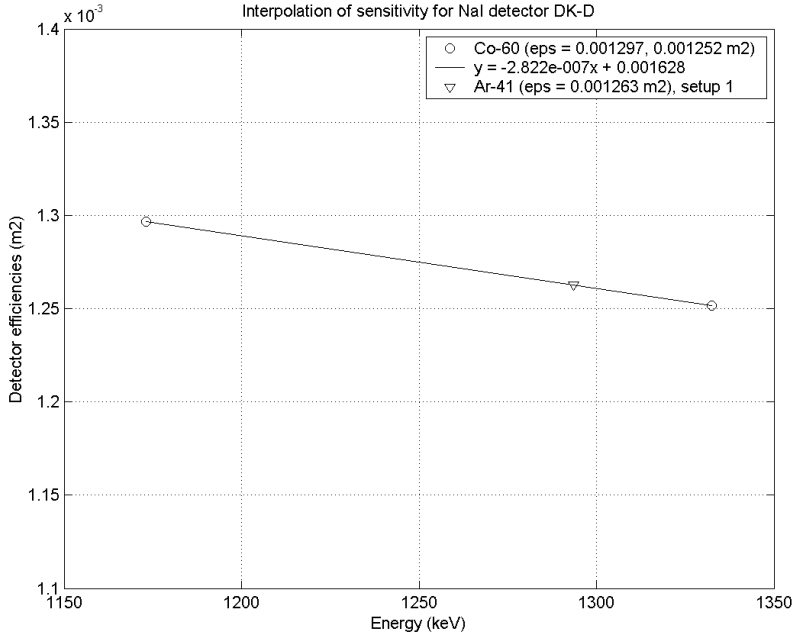

Figure 19. Detector efficiency for ^{41}Ar obtained by interpolation. Detector DK-D, setup 1.

Figure 20 shows ^{41}Ar primary photon fluence rates recorded Wednesday afternoon, using the efficiencies given in Table 5. The fluence rates are calculated for each detector, after a constant background has been subtracted from the measured count rates in the ^{41}Ar windows. Each point shown represents the result of a 30 second measurement; the variations are seen to be very fast. The four detectors shown were placed along a line roughly perpendicular to the plume centerline in the order: B, A, C, and D. The predominant wind direction was in the direction of detector B, as can easily be inferred from the figure. For the measurements of Wednesday morning the fluence rates of the DK-NaI detectors were found to coincide with those of the DTU-HPGe detector placed next to detector DK-B.

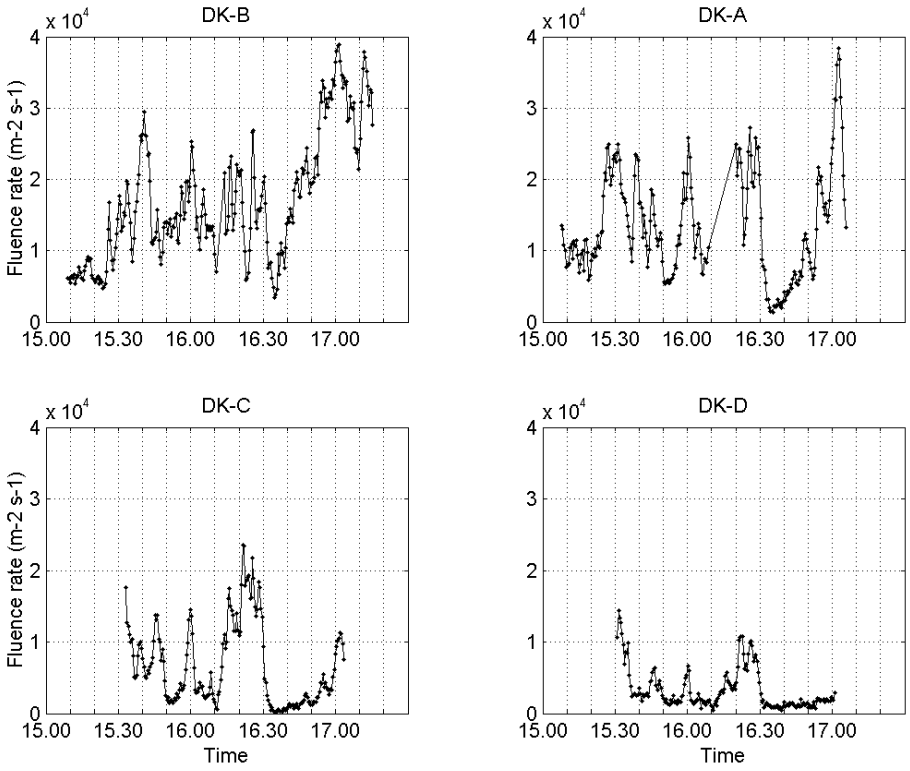

Figure 20. Fluence rate detected by the DK-NaI detectors on Wednesday afternoon.

5.1.2 SCK-NaI detector calibration

Providing a total count rate rather than full spectral information like the DK-NaI detectors, the SCK-NaI detectors do no discriminate between primary and Compton-scattered photons. Hence, the SCK-NaI detectors cannot be calibrated using only a point source since a point source at short distances gives rise to a smaller fraction of Compton-scattered photons than the extended argon plume. Instead, the SCK-NaI detector efficiencies were inferred from the intercalibration measurements of the SCK and DK NaI detectors. These measurements are described in more detail in section 7.1.

5.2 HPGe detectors

5.2.1 DTU-HPGe

The HPGe detector provided by DTU (referred to as DTU-HPGe) has an active volume of 148 cm^3 and 25 % efficiency (relative to a 3"× 3" NaI detector) for 1332 keV ^{60}Co.

The detector is controlled by EMCAplus software from SILENA, Italy. One of the features of this software is the possibility to run automatically controlled sequences of measurements. Each measurement is stored in a separate binary file with the start time included for identification of the measurement with respect to time. Earlier examinations of the angular efficiency of the DTU detector have shown that the efficiency is almost constant for all directions except for a 45° cone towards the dewar.

During the experiment, measurements were made with the detector at 1 m height above the ground, with the detector axis vertical and the crystal end pointing upwards. The automatic sequence function was used with set intervals of 5 minutes (2 minutes on October 4th) real

time measurements. Before the measurements were begun, the PC clock was synchronized to the meteorological data center clock time.
The energy calibration of the system is slightly temperature dependent, but can be approximated by

$$E(n) = [1.913 \cdot 10^{-7} \cdot n^2 + 1.557 \cdot n + 0.3079] \text{ keV},$$

where n is the channel number.

The HPGe detector was calibrated with a ^{60}Co point source at 1 m distance from the detector. The activity of the (Amersham) source was Q = 246.7 kBq (the DK-HPGe detector was calibrated a couple of days prior to the calibration of the NaI detectors). The primary photon fluence rate at distance R from the source is calculated as:

$$\varphi = Q \cdot y / (4\pi \cdot R^2) \qquad (1)$$

where y is the γ-yield and the attenuation in the air and the source encasing has been neglected. ^{60}Co has two full-energy gamma-lines at 1173.2 keV and 1332.5 keV, each with a yield of approximately 100%. An activity of 246.7 kBq therefore gives rise to a fluence rate, $\varphi = 19600$ m^{-2} s^{-1}, at the distance of 1 m.

Figures 21 and 22 show the ^{60}Co peaks measured with the DTU-HPGe detector. From the measured spectrum the laboratory background has been subtracted. The measurement time was 300 s in both cases. The full-energy-peak count rates were calculated as the sums of count rates in the channels from 749-759 (1173 keV) and 851-861 (1332 keV).

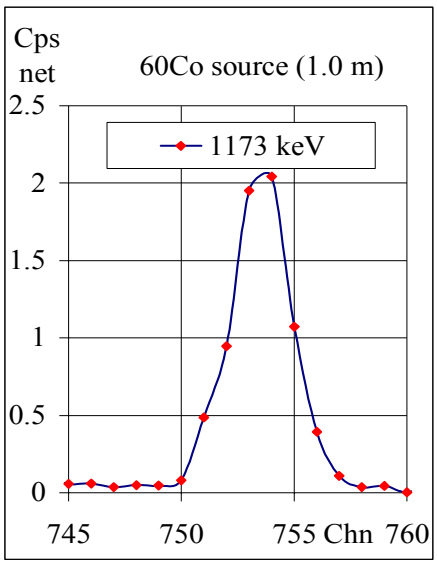

Figure 21. 1173.2 keV peak.

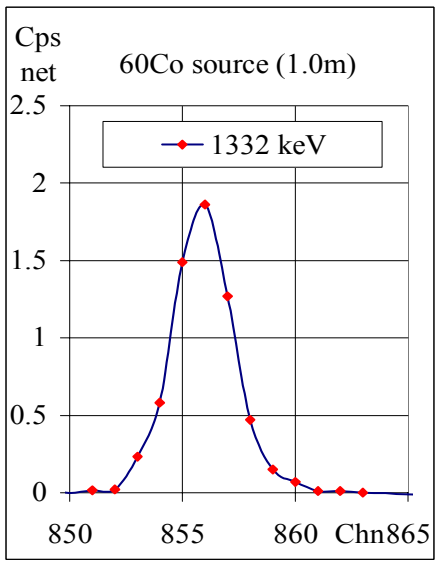

Figure 22. 1332.5 keV peak.

The detector efficiency is defined as r/φ, where r is the net window count rate for the full energy peak. The calculated values of r were 7.21 cps (1173.2 keV) and 6.17 cps (1332.5 keV). This yields

$$(r / \varphi)_{1173.2} = 3.67 \cdot 10^{-4} \text{ m}^2$$
$$(r / \varphi)_{1332.5} = 3.14 \cdot 10^{-4} \text{ m}^2.$$

^{41}Ar has a strong 1293.6 keV gamma line with a yield of 99.2 %. By linear interpolation, see Figure 23, between the detector sensitivities for ^{60}Co the detector efficiency for ^{41}Ar is estimated as

$$(r / \varphi)_{1293.6} = 3.28 \cdot 10^{-4}\ m^2.$$

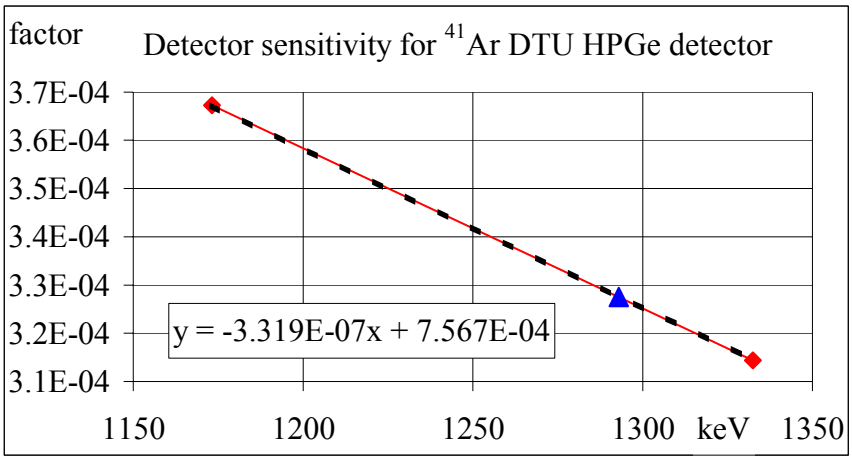

Figure 23. DTU-HPGe detector efficiency. ^{41}Ar represented by triangle.

Because of the influence from hardware warm-up every measured spectrum was plotted and the positions of the windows of interest were checked. In some cases it was necessary to move the window limits. For all valid measurements the window count rates were calculated.

Table 7. DTU-HPGe measurement information.

Date	Measurement start time, approx.	no. of valid measurements	Measurement time (s)	Filename
October 2	11:50	5	300	Fun
October 2	12:32	7	300	1Tu
October 3	10:02	29	300	1We
October 3	14:28	25	300	2We
October 4	10:52	63	120	1Th
October 4	13:26	88	120	2Th

Figures 24 to 27 show the primary photon fluence rates for ^{41}Ar. The data for October 2nd is not shown. In the figures the fluence rates were not corrected for background. The background was found to be very low due to low contents of natural radionuclides in the soil at Mol. The background count rate was estimated to 0.24 cps for the ^{41}Ar window (1293.6 keV γ-energy, channel interval 829-834), corresponding to a fluence rate of about 800 m^{-2} s^{-1}. Figure 28 shows an example of a full energy peak for ^{41}Ar (logarithmic scale). The dotted line indicates the background level.

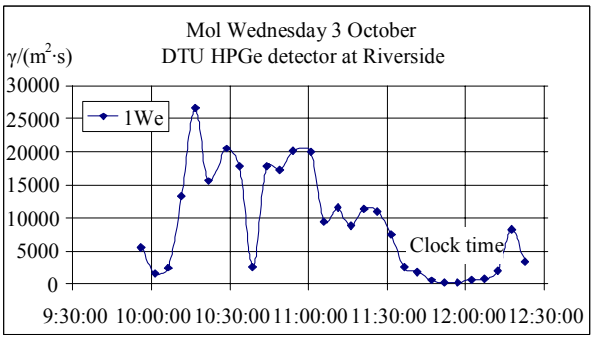

Figure 24. DTU-HPGe ^{41}Ar fluence rates.

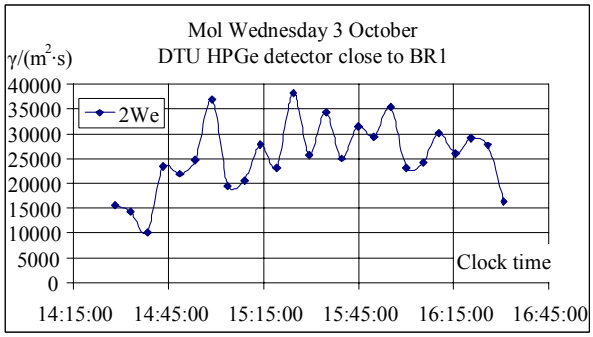

Figure 25. DTU-HPGe ^{41}Ar fluence rates.

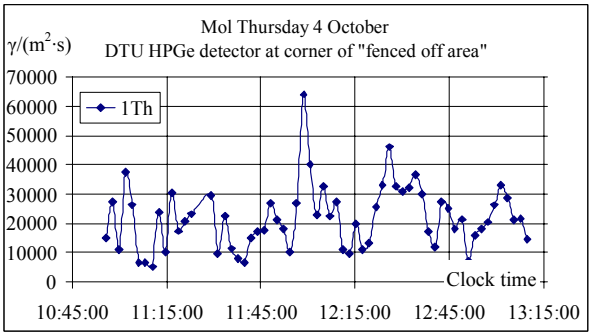

Figure 26. DTU-HPGe ^{41}Ar fluence rates.

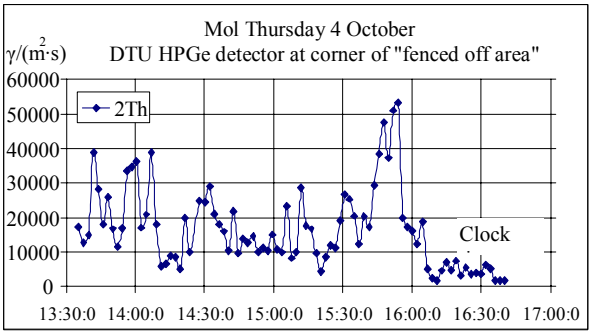

Figure 27. DTU-HPGe ^{41}Ar fluence rates.

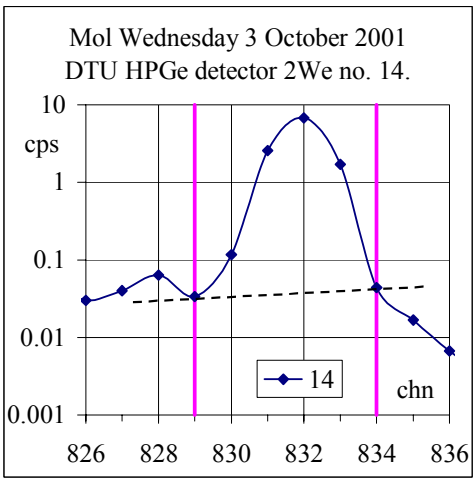

Figure 28. October 3rd, 2We sequence measurement no. 14 (5 min).

5.2.2 SCK-HPGe

The detector provided by the SCK•CEN is a HPGe detector n-type with an active volume of 55 cm³ and is 10.6 % efficient (relative to a 3" x 3" NaI(Tl) detector measured at 25 cm source – detector distance for a 1332.5 keV gamma-line from a ^{60}Co source). The full width half maximum (FWHM) is 1.79 keV at 1332.5 keV. The detector is manufactured by Canberra.

The acquisition and analyses software used is Genie-2000 (Canberra). Unlike the Danish system the software is not able to record automatic sequences. Each measurement has to be stored individually. All acquisition data are, however, automatically stored with the

measurement. The dispersion used is 1 keV/channel. The detector was energy-stable during the measurements and the gain factor did not need to be adjusted.
The detector was placed at 1.5 m above the ground, the axis vertical with the crystal end pointing upwards. Most of the measurements had a sampling time of 10 minutes after which the spectrum was saved and the next acquisition started. Before the measurements started, the PC clock was synchronized to the meteorological data center clock time. Figure 29 shows an example of a typical spectrum collected by the SCK-HPGe detector.

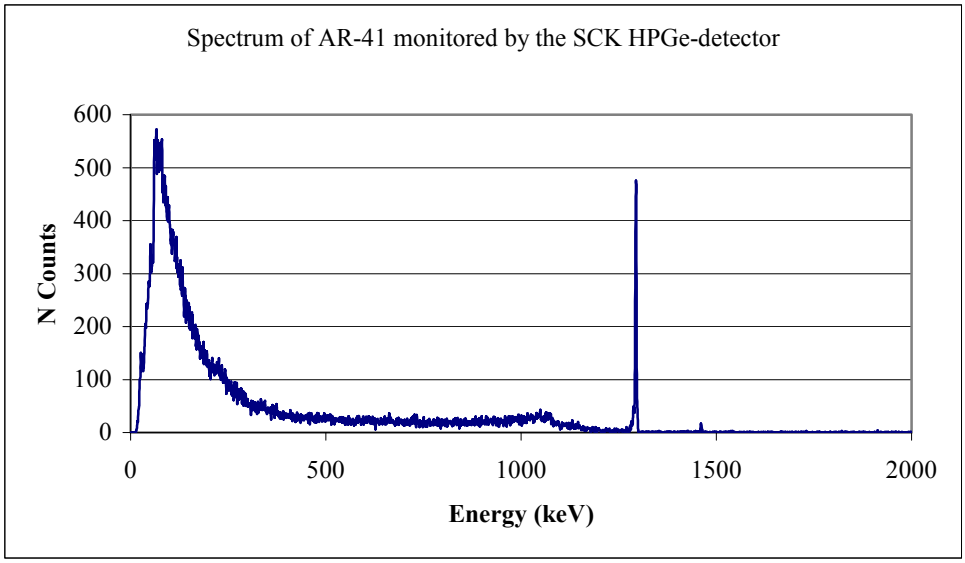

Figure 29. A typical spectrum from ^{41}Ar monitored by the SCK-HPGe-detector.

The detector efficiency was calibrated from the response to a ^{60}Co point source at 1 m distance from the center of the detector crystal. The activity of the cobalt source was measured to Q = 246.7 kBq on October 1st 2001, yielding the primary photon fluence rate, $\varphi = 19600\ m^{-2}\ s^{-1}$, at 1 m distance, cf. Eq. (1).

From the full-energy-peak count rates, r = 2.23 cps (1173 keV) and r = 1.95 cps (1332 keV), the detector efficiencies are obtained,

$$(r/\varphi)_{1173.2} = 1.14 \cdot 10^{-4}\ m^2$$

$$(r/\varphi)_{1332.5} = 0.99 \cdot 10^{-4}\ m^2.$$

We make the linear interpolation, cf. Figure 30, for ^{41}Ar (E = 1293.6 keV and y = 99.2%), to obtain the efficiency (Figure 30),

$$(r/\varphi)_{1293.6} = 1.04 \cdot 10^{-4}\ m^2.$$

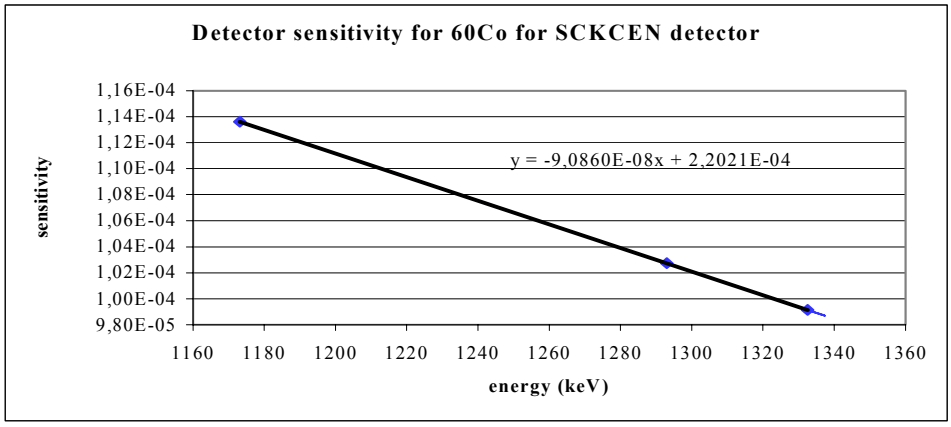

Figure 30. Detector efficiency for ^{60}Co for the SCK-HPGe detector.

Table 8. SCK-HPGe measurement information. "nn" is a file index number.

Date	Measurement start time, approx.	no. of valid measurements	Measurement time (s)	Filename
October 3	14:54	1	5722	Smoke*nn*0310
October 4	14:19	12	600	Smoke*nn*0410
October 5	9:30	15	600	Smoke*nn*0510

6 Plume measurements

6.1 Artificial smoke generation

The Risø smoke generator was positioned near the base of the BR1's 60-m stack, and a 25 cm Ø hose was inserted and raised to a height of about 30 meters. The hose was inserted in order to protect the stack's permanent monitoring instrumentation taken from a suction pipe at the 24-m level.

The smoke generator produced a continuous release of aerosols with typical aerodynamic diameters in the sub-micrometer range, consisting of a conglomerate of SiO_2 and NH_4Cl, which could easily be detected by the Lidar system. Mixing $SiCl_4$ and a 25% solution of NH_4OH in their neutralizing, stoichiometric ratio (1:3.2) in a strong air stream (jet), the two liquids react instantaneously:

$$SiCl_4 + 2H_2O \rightarrow SiO_2 + 4HCl,$$
$$NH_4OH + HCl \rightarrow NH_4Cl + H_2O.$$

Stable and strong artificial smoke plumes were in this way generated for the experiments. In-situ measurements of the size distributions of the artificial smoke particles, taken from both the plume's centerline and from its sides, turned out to be remarkably constant with respect to both time and shape.

Figure 31. Mixing of chemicals for aerosol production.

6.2 The Risø Mini Lidar Systems for smoke-plume scanning

With the purpose of obtaining detailed measurements of the instantaneous cross-wind concentration profiles within smoke plumes, Risø in the late 80'es built a high-resolution aerosol-backscatter Lidar system based on a coaxial laser/receiver configuration introduced by the German Aerospace Centre DLR [5-7].

The ground based Risø Mini Lidar system is used to quantify aerosol concentrations in the atmosphere. It is sensitive enough to detect natural occurring aerosol backscatter from single laser shots in the range 50 - 500 m. During controlled diffusion tests, however, it measures backscatter from artificially generated smoke puffs and plumes, which we turn into calibrated aerosol concentrations, see below.

The Risø mini -Lidar system consists of:

- A pulsed laser system (water cooled)
- A Cassegrain telescope with filters and detectors
- A digital sampling/storage scope
- A stepper motors with controllers for scanning (azimuth and declination)
- A PC control and data acquisition and storage system
- A mini Van (Ford Transit)

Figure 32. The Risø Lidar bus.

The Lidar principle of operation is much like conventional radar except that it uses a pulsed infrared laser beam instead of radio waves. A short light pulse is emitted by the laser and the echo is recorded by the storage scope. The aerosol positions are given by the time delay of the echo and the strength of the echo is related to the aerosol particle concentration at that position (see below). From a single laser pulse, typically 500 simultaneous sampling points (range gates) are recorded along the beam path. The detector and the laser beam are built coaxial in the telescope. The telescope with laser head and detector can be turned along two axes (azimuth and declination) by means of stepper motors, cf. Figure 32.

The Lidar head with telescope, detector and laser head can scan vertically between two pre-set turn angles in order to scan cross-sections of continuous smoke plumes. Each vertical scan consists typically of 20 laser shots covering angles between 0° and 20°. A scan typically lasts 1 sec with 20 or 40 rays covered per scan. The turn around time is approximately 1.5 sec between the scans. The pause is used to decelerate and accelerate the telescope and to transfer data to the PC.

During continuous smoke plume experiments, the radial distance between range gates is 0.75 m (sampling rate 200 mega-samples/s). This corresponds to a Nyquist sampling length of 1.5 m consistent with the overall spatial bandwidth of the detector system (see Table 9).

Range gates separation as small as 37.5 cm (400 mega-samples/s) can be achieved, and smoke plumes can be scanned at distances from ~100 m in front of the Lidar head up to distances several kilometers away. Typically in experiments with artificial smoke, plumes are scanned or measured at distances ranging from 200 to 800 m from the laser head.

Table 9: The Risø Mini-Lidar systems technical specifications.

Laser:
Flashlight pumped Nd:YAG Model U-FR100 wavelength 1064 nm from Big Sky Laser Company, MN, USA, Energy 3-14 mJ/pulse, pulse length (Q switched) ~10 ns; repetition rate 55 Hz. Full-angle divergence ~3 mrad.
Telescope:
Folded two-mirror Cassegrain from IBS GmbH, Germany; 15 cm Ø - effective area ~144 cm^2. Full-angle field of view 10 mrad with laser line interference filter @1064 nm; FWHM 10 nm; peak transmittance 45%.
Detectors:
Type 1) YAG 444 Silicon photo diode; sensitivity 45 A/W @ 1064 nm; rise time < 9 ns, + 20 dB preamplifier (AD9611 w/ 280 MHz 3 dB point bandwidth).
Type 2) Wide band silicon avalanche photo diode with hybrid pre-amplifier module (EG&G type C30950E; System bandwidth 3 dB point 200 MHz, responsivity @ 1064 nm $1.4x10^5$ Volt/Watt.
Data sampling:
LeCroy Digital Oscilloscope model 9450A with 300 MHz bandwidth; 400 mega-samples/s single shot sampling rate (corresponding to spatial sampling intervals of 37.5 cm).
Lidar systems overall effective spatial resolution[1]:
Impulse half-width response ~ 10 ns corresponding to effectively 1.5 m bandwidth (3 dB point).
Lidar systems time resolution
500 simultaneous range gates sampled at 55 Hz. (Burst mode)
Lidar systems maximum data throughput
500 simultaneous range gates averaged over 4 shots at 8 HZ
Scanning: 20° scan angle w / 0.5° resolution scanned with 40 Hz rep. rate (up and down).

6.2.1 From Lidar returns to aerosol concentrations

A short light pulse with high energy (effectively ~1.5 m long with energy 10 mJ is emitted from the laser head and fed into the Lidar systems coax centerline. The backscatter from aerosols in the beam path is then detected and digitized by the scope.

[1] Estimated from hard target backscatter profiles, i.e., including the effective broadening from finite laser pulse length, detector bandwidth, preamplifier bandwidth and data acquisition systems (oscilloscopes) response time.

The interpretation of Lidar returns in terms of aerosol concentrations are based on the theory of propagation of electromagnetic radiation and attenuation in an optically dense media. The distance r from the Lidar head to the aerosols is given by the time delay of the echo for each range gate. The strength of the echo at range r, the received power $P(r)$, is related to the aerosols effective volumetric backscatter coefficient $\beta(r)$ through the Lidar equation,

$$P(r) = P_o \left(\frac{c\tau}{2} \right) F(r) \; A_t \; \frac{1}{r^2} \beta(r) \; e^{-2\int_{r_0}^{r} \kappa(r')dr'} , \qquad (2)$$

where $P(r)$ is the power received from the range $r = ct/2$, where c is the speed of light and t is the echo time. P_o is the power transmitted at time zero. The effective length of the laser pulse is $c\tau/2$, where τ is pulse duration of the laser. A_t is the effective area of the telescope, and divided by r^2 this term defines the solid angle acceptance. The design with the laser pulse emitted in front of the telescope (coaxial) results in a simple geometric transmitter/receiver overlap function, $F(r)$, which accounts for the effective overlap of the receivers field of view with the laser pulse. (This factor is only of importance at the shortest ranges, r <100 m.)

$\beta(r)$ [Sr^{-1} m^{-1}] denotes the volumetric (per unit volume) backscatter coefficient of the atmosphere at range r, and $\kappa(r)$ [m^{-1}] is the corresponding extinction coefficient.

The volumetric backscatter coefficient defines the fraction of incident energy scattered per solid angle in the backward direction (180°) per unit length. The volume extinction coefficient κ defines correspondingly the fraction of the energy flux that is lost per unit length during the propagation.

In general, both the backscatter and the extinction properties depend on wavelength, particle size, and the optical properties of the aerosols. The Lidar equation (2) applies to relatively transparent medium where only single-scattered light is accounted for. The Lidar equation therefore relates the backscatter and extinction coefficients range dependency to the Lidar return signal $P(r)$, and the optical geometry of the transmitter and receiver units

.

Given a measured Lidar return profile, $P(r)$, the Lidar equation (2) becomes a first order integral equation with two unknown quantities, $\beta(r)$ and $\kappa(r)$. In order to solve this equation, a linear relationship between $\beta(r)$ and $\kappa(r)$ is introduced, based on Mie-scatter theory as applied to elastic scattering on spherical particles. This complements the Lidar equation.

For single-scatter processes, the backscatter coefficient is proportional to the number of particles per unit volume, that is, to the particle density. Puff or smoke plume internal aerosol concentrations can therefore, to first order, be interpreted as being proportional to the Lidar systems inferred backscatter coefficient $\beta(r)$, provided that the optical properties of the aerosols (e.g. the smoke particle size distribution) will not change during measurement trials (½-1 hr).

During stationary meteorological conditions with respect to background aerosol level and humidity, we assume that the particle size distribution is constant, and consequently proportionality between backscatter and aerosol concentration is obtained.

6.2.2 Data processing and calculated plume parameters

The Lidar scanned 50 lines within a specified angle interval in each of the experiments performed during the experiment. The scanning velocity was in the order of 20-30

degrees/sec, and the interval between each scan was of the order of 2 or 3 seconds depending on the angle interval. In each of the lines the extinctions $\kappa(r)$ was calculated based on the solution to the Lidar equation (2) given by

$$\kappa(r) = \frac{S(r)}{\frac{S(r_0)}{\kappa_0} - \int_{r_0}^{r} S(r')\mathrm{d}r'},$$

where *S(r)* is the normalized Lidar return:

$$S(r) = \frac{P(r)}{r^2 K_{sys}},$$

and where K_{sys} is the system constant including telescope area and emitted power. The calculations start from r_0 equal to approximately 30 meter to reduce effects from the overlap function $F(r)$. For each experiment we have calculated the mean crosswind plume profile of extinctions as:

$$\overline{\kappa(\theta, r)} = \frac{1}{N}\sum_{i=1}^{N} \kappa(\theta(t_i), r(t_i)),$$

where $\kappa(\theta(t_i),r(t_i))$ is the extinction as function of angle $\theta(t_i)$ to the time t_i and the range r . The average profile of extinctions $\overline{\kappa(\theta, r)}$ is interpolated into a rectangular grid $\overline{\kappa(y, z)}$ by a linear area interpolation.

The extinctions are assumed to be equal to concentrations whereas the calibration factor between the measured extinctions and smoke particles is unknown. In the following we write the extinctions as $c(y,z)$. The dispersions parameters such as the spread σ_z , σ_y and the centerline positions y_c, $\overline{Z}$ are calculated based on the crosswind integrated profiles of $c(y,z)$,

$$y_c = \frac{\int y \int c(y,z)\mathrm{d}z\,\mathrm{d}y}{\iint c(y,z)\mathrm{d}z\mathrm{d}y}$$

$$\overline{Z} = \frac{\int z \int c(y,z)\mathrm{d}y\,\mathrm{d}z}{\iint c(y,z)\mathrm{d}z\mathrm{d}y}$$

$$\sigma_y^2 = \frac{\int (y-y_c)^2 \int c(y,z)\mathrm{d}z\,\mathrm{d}y}{\iint c(y,z)\mathrm{d}z\mathrm{d}y}$$

$$\sigma_z^2 = \frac{\int (z-\overline{Z})^2 \int c(y,z)\mathrm{d}y\,\mathrm{d}z}{\iint c(y,z)\mathrm{d}z\mathrm{d}y}$$

6.3 Examples of plume scans

Figure 33 shows an example of a plume scanning sequence obtained in the morning of Friday October 5th 2001. These scans were obtained along the "channel" and just over the gamma detectors (cf. Figure 15).

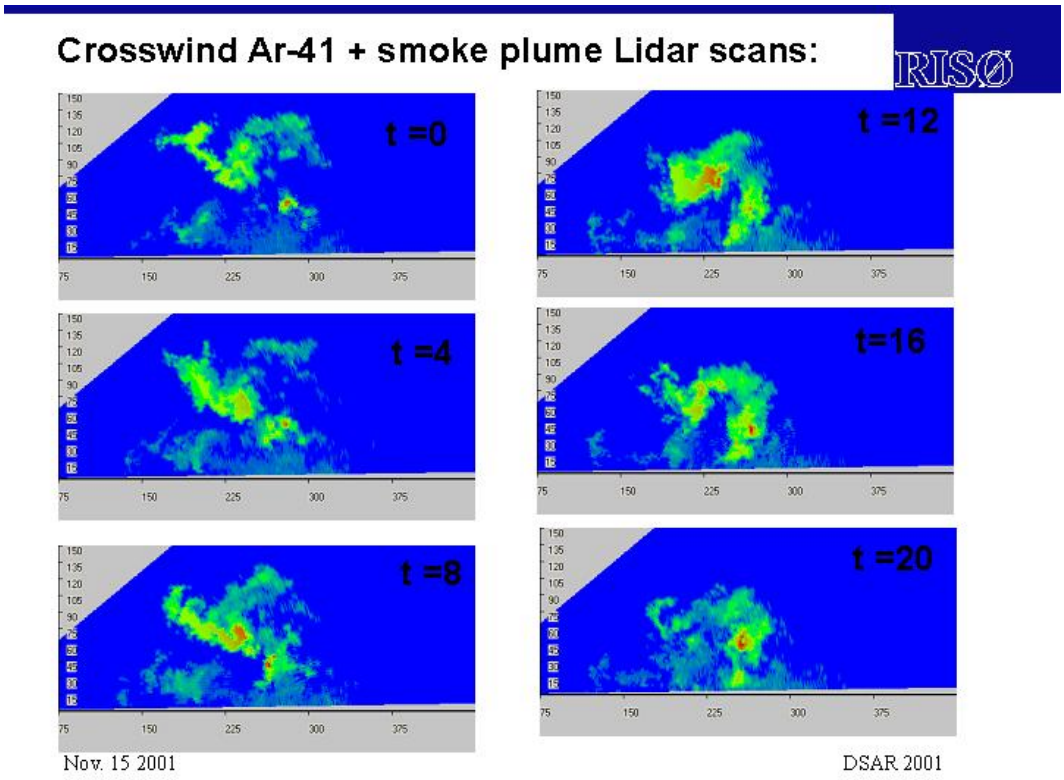

Figure 33. Crosswind smoke plume scanning sequence of 20 s, obtained in the morning of Friday October 5th 2001.

The corresponding mean crosswind concentration profiles $\overline{c(y,z)}$ and crosswind integrated profiles $\overline{c_z(y)}$ and $\overline{c_y(z)}$ are shown in the Figures 34-36.

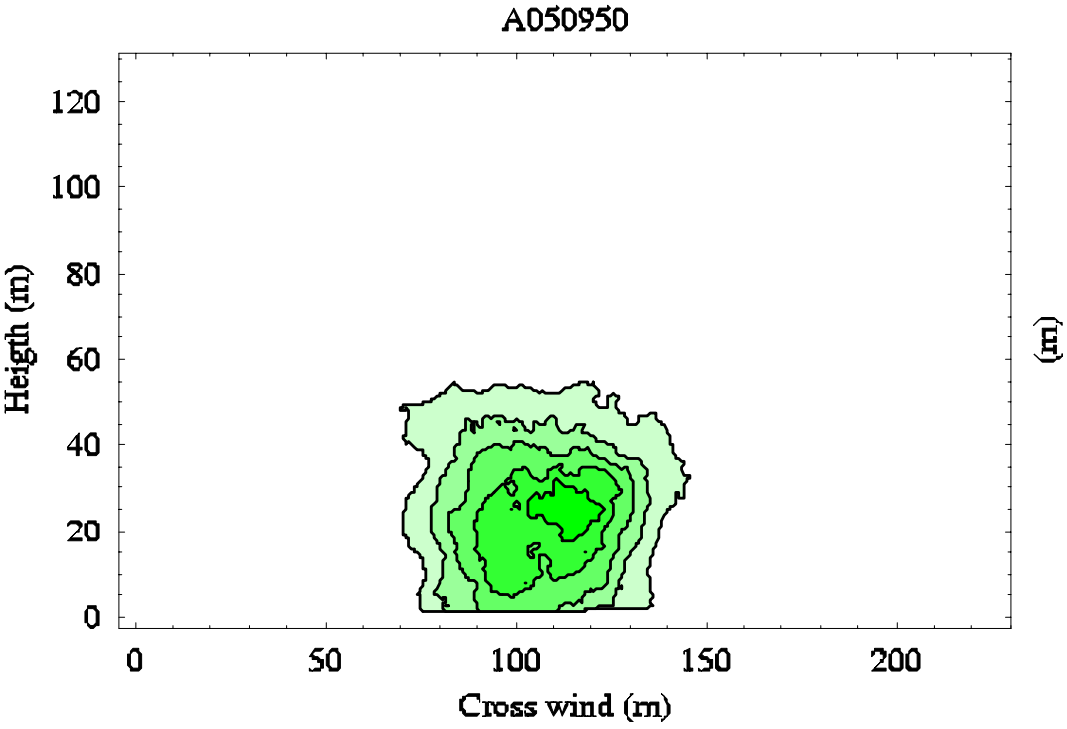

Figure 34. Cross wind integrated mean concentration profile.

Figures 35-36 show the cross wind integrated profiles on which the calculation of the dispersion parameters are based.

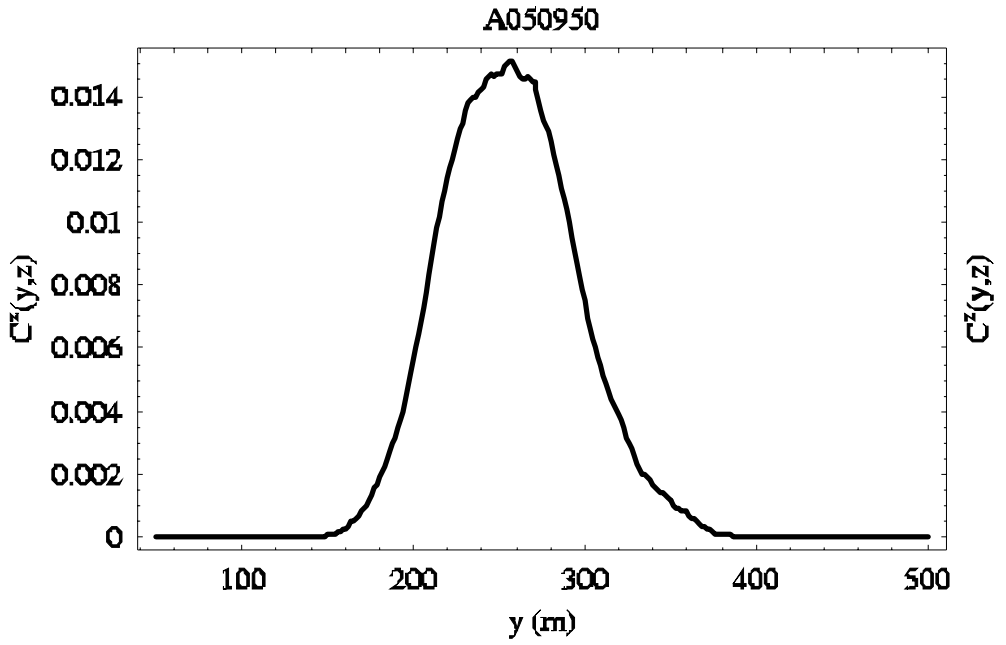

Figure 35. Crosswind integrated mean profile $\overline{c_z(y)}$

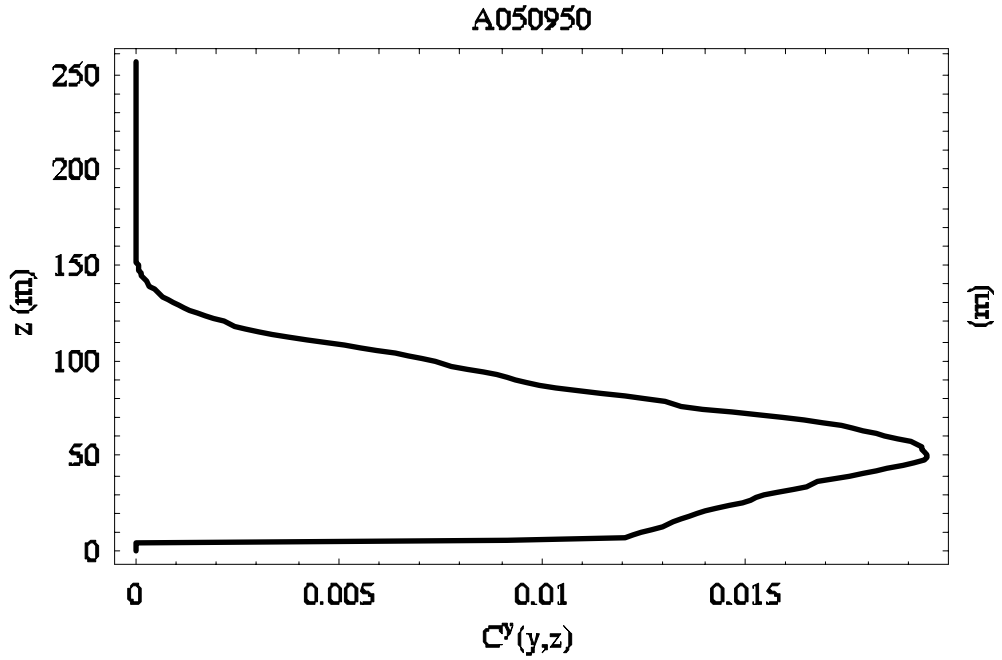

Figure 36. Crosswind integrated mean profile $\overline{c_y(z)}$.

7 Spectral data processing

7.1 Inter-calibration of NaI detectors

Using two different kinds of NaI detectors for this experiment, one series of measurements (in the afternoon of October 3rd) was performed specifically in order to allow correct inter-calibration of the two detector arrays. During these measurements, the eight NaI detectors were placed pair wise, one from the SCK-NaI detector array and one from the DK-NaI detector array, cf. Figure 7.

The results of the inter-calibration are shown in Figure 37. The scatter plots show simultaneous values of the total count rates obtained by a SCK-NaI detector and the ^{41}Ar primary photon fluence rates measured by the corresponding DK-NaI detector. The latter were calculated from the background subtracted count rates using the efficiencies of Table 5. For three of the four detectors, the plots show a strong correlation, while for detectors DK-D and SCK-1 the correlation is poor. The slope of the linear regression gives the efficiency of the SCK-NaI detector; the background level is found from the intersection with the y-axis. The results are summarized in Table 10. The count rates of the SCK-1 detector differ from those of the other detectors, indicating that a different threshold was set for this detector. However, the poor correlation observed on Figure 37 implies that the results obtained with the SCK-1 detector are more uncertain.

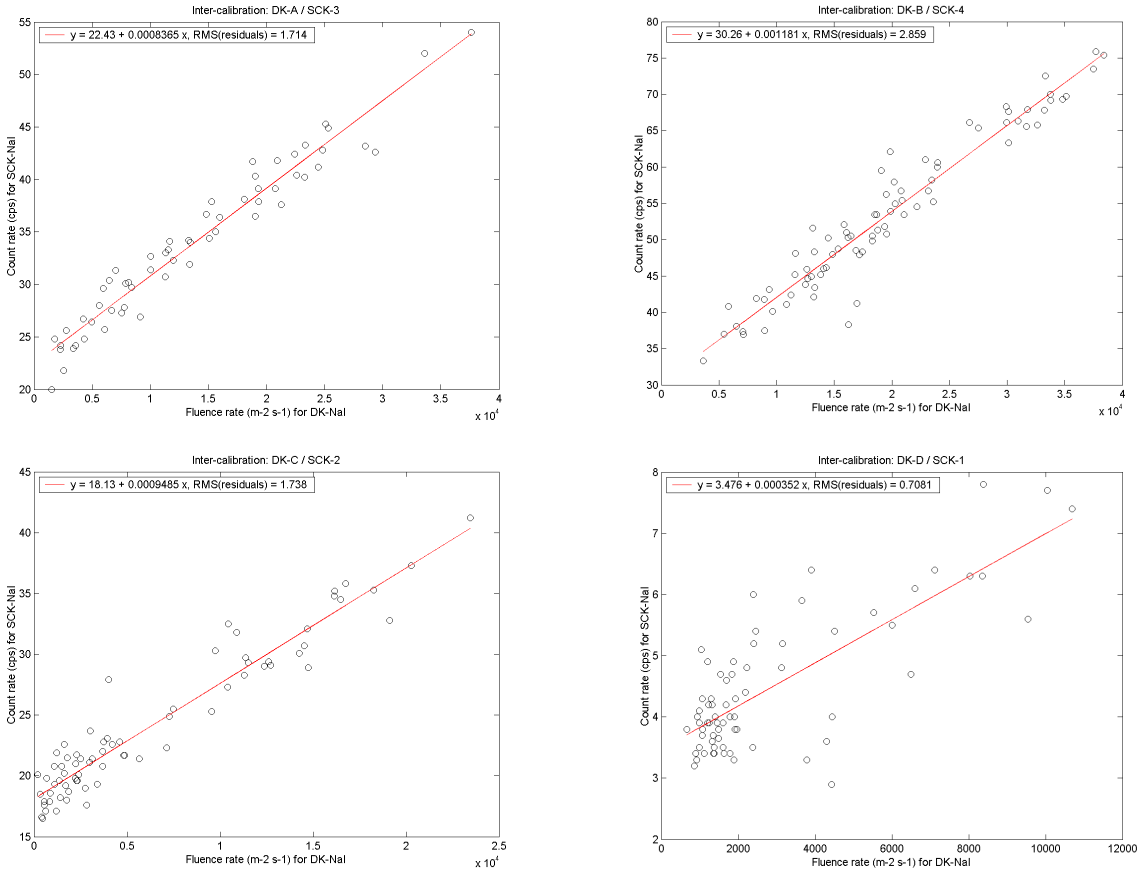

Figure 37. Inter-calibration of NaI detectors.

Table 10. Detector efficiencies and window background fluence rates for SCK-NaI detectors.

Detector	ε (m^2)	$\varphi_{background}$ (m^{-2} s^{-1})
SCK-1	0.000352	9900
SCK-2	0.000949	19100
SCK-3	0.000837	27000
SCK-4	0.001181	26000

7.2 Noise Adjusted Singular Value Decomposition

When a radioactive source exposes a NaI detector from different distances, one observes that the spectral shape varies, as the general amplitude of the spectra is strongly dependent on the distance due to the r^{-2} effect and attenuation in the air. A detailed examination of the spectral shape unveils that the ratio between the full energy peak count rate and the background-subtracted count rate at the lowermost energies decreases with increasing distance. The reason is that Compton scattering in air reduces the fluence rate of primary photons but generates lower energy photons. Therefore the fluence rate of low energy photons caused by the presence of the source is relatively higher at larger distances from the source.

During the measurements of ^{41}Ar from BR1, the distance between the plume and the NaI detectors varied considerably. In addition to the variation in total intensity, which can be represented by a count rate of a spectral window around the full energy peak of ^{41}Ar, one should thus be able to observe a varying spectral shape caused by Compton scattering of photons from the plume.

The most effective way of getting quantitative information on the spectral shape of spectra from NaI detectors is to perform a Noise Adjusted Singular Value Decomposition (NASVD) of the set of spectra [8, 9]. In short, this technique examines the common variations within the set of spectra, generating a number of spectral components that can be used for a reconstruction, partial or complete, of all spectra in the set. Denoting the spectral components $\mathbf{s}_i$, the reconstructed spectra are given by

$$\mathbf{r}_j = \mathbf{s}_0 + (\mathbf{s}_1 b_{1j} + \mathbf{s}_2 b_{2j} + \cdots + \mathbf{s}_n b_{nj})/T_j, \qquad (3)$$

where the index j is the spectrum number, T_j is the live time, and the amplitudes b_{ij} are fitted for each spectrum. The NASVD technique calculates the spectral components $\mathbf{s}_i$, such that as few spectral components as possible are needed in order to allow all measured spectra in the set to be reasonably approximated by the reconstructed spectra $\mathbf{r}_j$. In Equation (3), $\mathbf{s}_0$ denotes the average spectrum, while for the present case $\mathbf{s}_1$ may be identified as an average ^{41}Ar spectrum. The spectral component $\mathbf{s}_2$ will have a positive signal in the full energy window of ^{41}Ar and a negative signal at the lowermost energies - or vice versa.

When considered together, b_1 and b_2 contain information on the total amount of ^{41}Ar in the plume and the mean distance from the detector, hence both should be included in an evaluation. A high value of b_1 can be due to a small amount of ^{41}Ar close to the detector or a large amount of ^{41}Ar at a larger distance. The value of b_2, however, will tell which of the possibilities is the actual case.

In order to evaluate the possibilities for extracting this type of information from the time series of spectra measured in the Mol experiment, a few of the series have been examined with the program NUCSpec [10] that *inter alia* includes the possibility for NASVD

processing. Below some of the results are described for processing of data from Thursday morning with the DK-A detector placed at the north-western fence of the SCK•CEN area (see Figure 5).

Figure 38 shows the "rainbow plot" and spectrum 67. The peak, which is centered at channel 217, is due to full energy detections of 1293.6 keV photons from ^{41}Ar. From the spectrum, it is found that the argon signal dominates the spectrum. Furthermore, at channel 245, a weak peak due to natural ^{40}K is observed. In the "high energy part" of the spectrum few counts caused by thorium and uranium decay products are noticed. The natural background level at SCK•CEN is very low, due to the high content of pure quartz sand in the upper part of the ground.

In the rainbow plot a strongly varying argon signal is observed, making the data ideal for extracting different argon spectra with the NASVD technique.

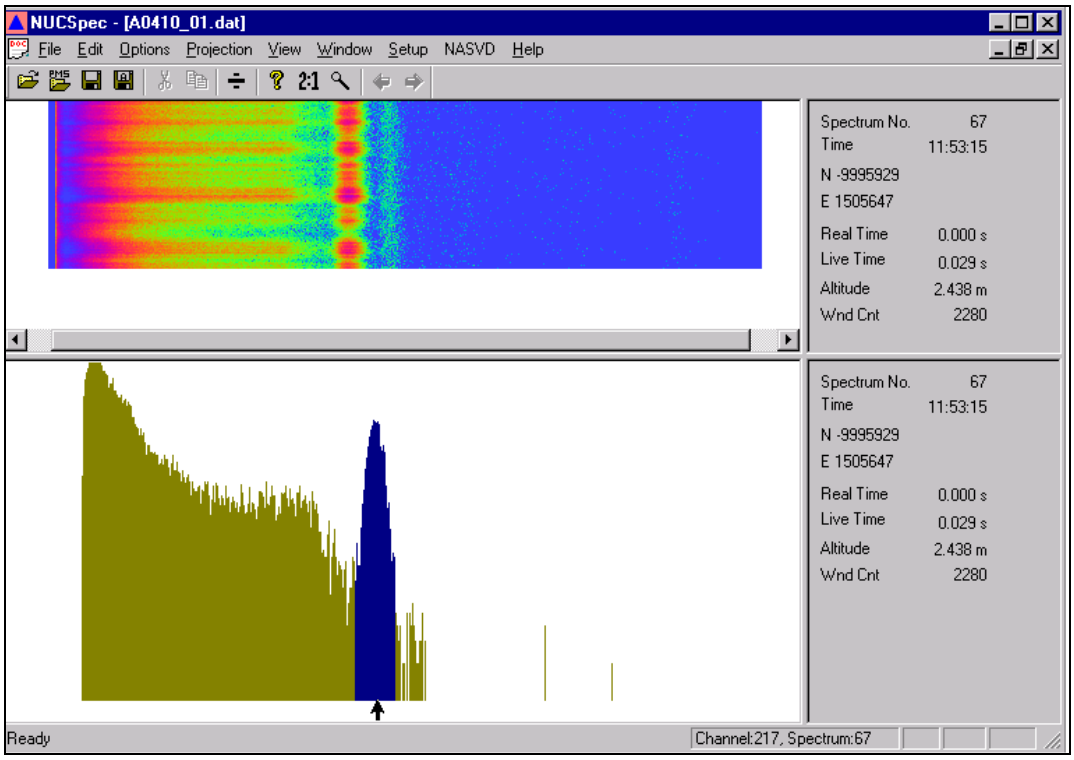

Figure 38. NUCSpec 2.1. Spectra measured with DK-A.

The NASVD processing was done based on the channels 20 to 240; the result is shown on Figure 39, picturing the mean spectrum and the spectral components s_1 and s_2. The mean spectrum is dominated by the ^{41}Ar signal. However, at the lowermost energies one notices multi-scattered photons from natural background. Spectral component $\mathbf{s}_1$ is a pure ^{41}Ar spectrum. One notices the full energy peak of argon around channel no. 217 and the Compton plateau between the channels 100 to 170. Probably there is some forward-scattered radiation detected in the Compton valley between the channels 190 and 200. At the channel numbers smaller than 100, argon photons are detected that have been Compton scattered one or several times in the air or in the ground. At channels 33 to 38, a minor peak is noticed. It is the ordinary backscatter peak at 214 keV from Compton scattering in the ground around the detector. Spectral component $\mathbf{s}_2$ is a typical “depth spectrum”, with a negative full-energy peak and a positive signal at the lowermost energies.

The spectral component no. 3 (not shown) contains a little spectrum drift and statistical noise. The remaining spectral components only contain statistical noise and should therefore not be included in the reconstruction of measured spectra. All the information that can be extracted from the measured spectra is included in the spectral components shown in Figure 39.

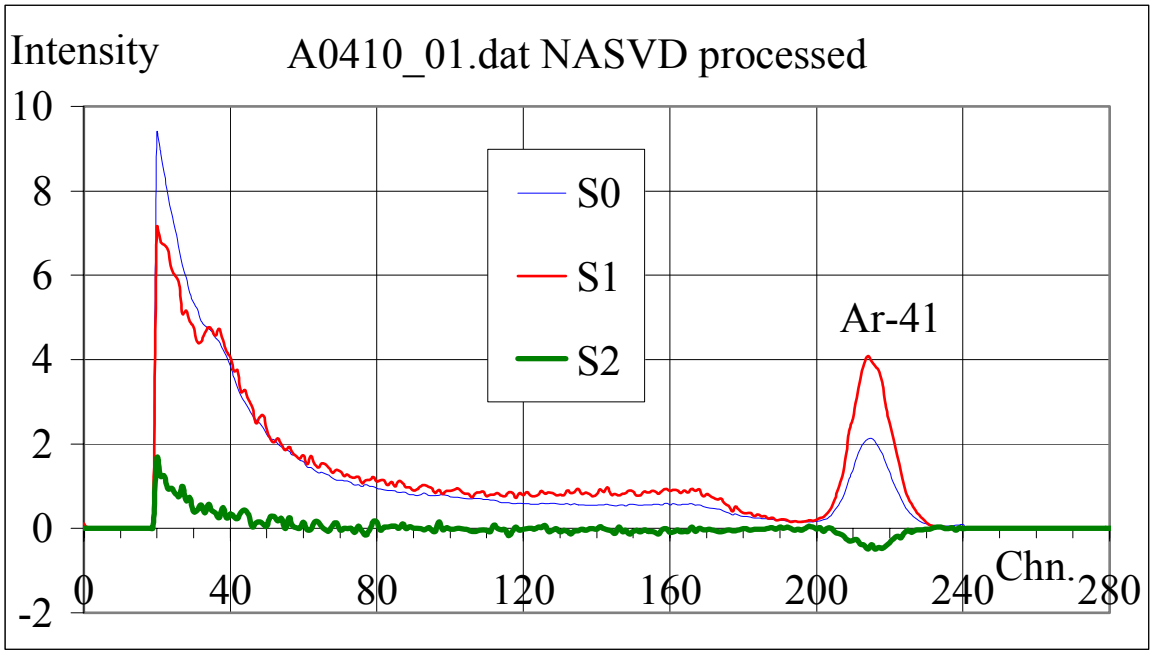

Figure 39. Mean spectrum, first and second spectral component for A0410_01.dat.

Figure 40 shows the amplitudes b_1 and b_2 for all the 120 spectra in the data set. One notices a large variation of both b_1 and b_2 indicating that the argon plume has had a varying position relative to the detector. The ratio b_2/b_1 is an indicator of the distance between the detector and the source: A large value b_2 will imply that the reconstructed spectrum contains less full energy counts (note the negative "full energy peak" of $\mathbf{s}_2$ in Fig. 38) and more low energy counts, corresponding to radiation from argon that is far away from the detector.

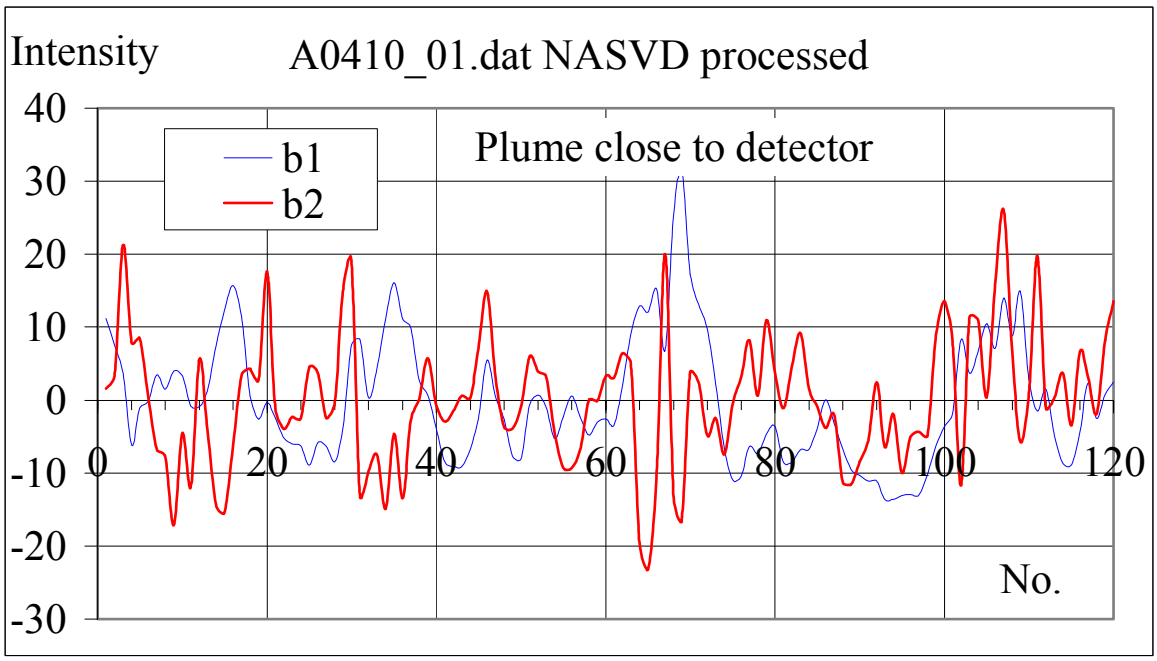

Figure 40. Amplitudes b_1 and b_2 of the spectral components $\mathbf{s}_1$ and $\mathbf{s}_2$, respectively.

Figure 41 shows the mean spectrum (also shown in Figure 39) together with the spectrum corresponding to natural background. There is a cut-off at channel 240. Therefore the (small) full energy peak at channel 245 due to ^{40}K is not seen. The "natural background spectrum" has been generated by subtracting a fraction (0.52) of $\mathbf{s}_1$ from the mean spectrum - with the goal of producing a spectrum without argon signal. One notices a very low-level background spectrum and a ^{41}Ar spectrum of a very different shape. This indicates that useful information can be extracted from the measured spectra.

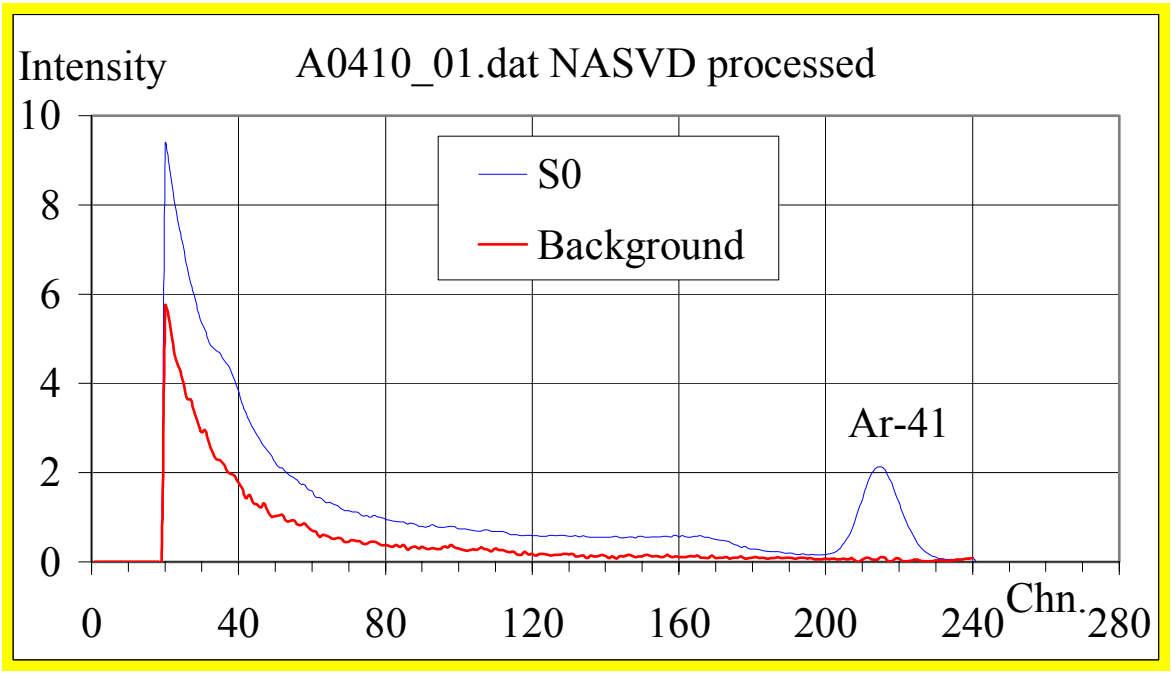

Figure 41. Mean spectrum and “natural” background spectrum.

In Figure 42, the differences between reconstructed spectra and the average spectrum, $\mathbf{r}_j - \mathbf{s}_0$, are shown for spectrum no. 69 and no.107. Spectrum no. 107 has been multiplied with a factor of 2.1 in order to get comparable spectrum count rates. If the natural background radiation is constant, it will only contribute to the average spectrum $\mathbf{s}_0$, but not to the difference spectra shown. One notices that the (adjusted) spectrum 107 contains less full energy events but more low energy events than does spectrum 69. The reason for having fewer full energy counts in spectrum 107 is that the average distance to the source atoms (^{41}Ar in the plume) has been larger for this spectrum than for spectrum no. 69.

In Figure 43 the simple window count rates for the measured spectra are shown. One notices that the variations of the window count rates closely follow that of the coefficient b_1. However, a close examination tells that there are minor differences - as there should be.

The examination of the NaI(Tl) spectra by the NASVD technique has shown that the spectra contain information on both primary photon fluence rates at the detector and on the mean distance between the source (^{41}Ar in the plume) and the detector. Due to a very low level of natural radioactivity and a strong ^{41}Ar signal, the data are of high quality. Therefore the results of the NASVD processing offer an independent way of assessing the spatial distribution of ^{41}Ar in the air.

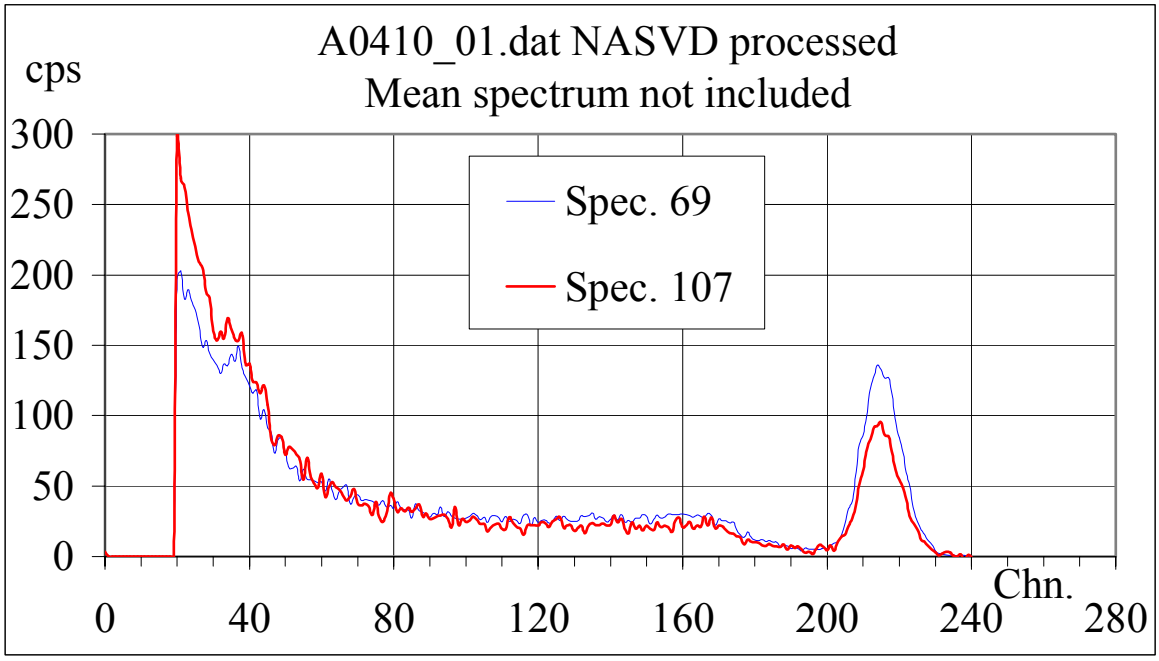

Figure 42. Difference between reconstructed spectra and mean spectrum, $\mathbf{r}_j - \mathbf{s}_0$, for j = 69, and j = 107.

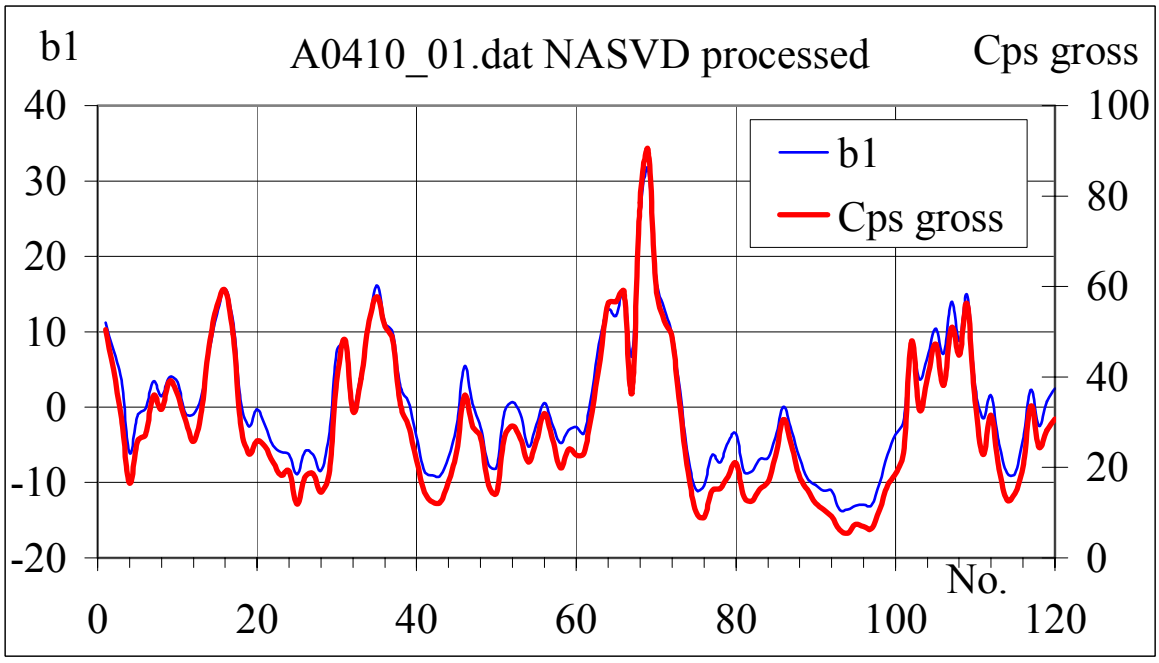

Figure 43. Gross window count rates (channel 201-229) for the measured spectra and amplitude b1 from NASVD processing of the data.

8 Conclusions

The Mol ^{41}Ar experiment was carried out with the purpose of obtaining data for the testing and development of radiological decision support tools. In particular, the objectives for obtaining data were to:

1. Evaluate atmospheric gamma dose-rate modules

Evaluation of the near-range gamma dose-rate modules in atmospheric dispersion models such as RIMPUFF, and

2. Evaluate practical data assimilation

Obtaining data suitable for evaluation of on-going research regarding data assimilation models on atmospheric dispersion, filtered with real-time gamma dose-rate measurements.

Re: 1. The data sets obtained are suitable for evaluation of atmospheric dispersion dose rate models, for which the source term and meteorological data are known input parameters.

Re: 2. The same data set can also be used in the testing and development of data assimilation models for real-time source term estimation. Measured meteorology and radiation monitoring data are here input parameters and the aim is to assimilate the plume geometry and the plume content, e.g. based on Kalman filtering. In this way it is possible to improve the estimate of the source term directly while the accident evolves (i.e., in the early phase), leading to improved dose assessments for decision support.

In the experiment simultaneous measurements were performed of the ^{41}Ar radiation field and plume dispersion of a visible tracer, in addition to meteorological and ^{41}Ar source term measurements. The complete data set has been organized into a database, and provides a unique opportunity for further analysis and modeling. The next scientific task is to make best use of these experimental data, to improve our capability for making better early phase prognoses of dose levels following a nuclear accident. Applied to decision support systems, this will allow for the advance introduction of adequate intervention measures to reduce radiation exposure of humans.

Acknowledgements

The authors are grateful to Jan Nielsen, Risø National Laboratory, and Willy Geenen and Simon Coenen, SCK•CEN, for their valuable assistance during the experiment

References

1. Mikkelsen, T.; Larsen, S.E.; Thykier-Nielsen, S.: Description of the Risø Puff Diffusion Model. Nucl. Technol. 67 (1984) 56-65.

2. Brandt, J.; Mikkelsen, T.; Thykier-Nielsen, S.; Zlatev, Z.: The Danish Rimpuff and Eulerian Accident release model (The DREAM). Phys. Chem. Earth (1996) **21** , 441-444.

3. Mikkelsen, T.; Thykier-Nielsen, S.; Astrup, P.; Santabárbara, J.M.; Sørensen, J.H.; Rasmussen, A.; Robertson, L.; Ullerstig, A.; Deme, S.; Martens, R.; Bartzis, J.G.; Päsler-Sauer, J.: MET-RODOS: A comprehensive atmospheric dispersion module. Radiat. Prot. Dosim. (1997) **73**, 45-56.

4. Astrup, P.; Mikkelsen, T.; Deme, S.: MET-RODOS: Meteorological pre-processor chain. Phys. Chem. Earth B (2001) 26 (no.105-110).

5. Jørgensen, H.E.; Mikkelsen, T.; Streicher, J.; Herrmann, H.; Werner, C.; Lyck, E., Lidar calibration experiments. Appl. Phys. B (1997) 64, 355-361.

6. Jørgensen, H.E.; Mikkelsen, T.: Lidar measurements of plume statistics. Boundary-Layer Meteorol. (1993) 62, 361-378.

7. Cionco, R.M.; Kampe, W.; Biltoft, C.; Byers, J.H.; Collins, C.G.; Higgs, T.J.; Hin, A.R.T.; Johansson, P.E.; Jones, C.D.; Jørgensen, H.E.; Kimber, J.F.; Mikkelsen, T.; Nyren, K.; Ride, D.J.; Robson, R.; Santabarbara, J.M.; Streicher, J.; Thykier-Nielsen, S.; Raden H. van; Weber, H.: An overview of MADONA: A multinational field study of high-resolution meteorology and diffusion over complex terrain. Bull. Am. Meteorol. Soc. (1999) 80, 5-19.

8. Hovgaard, J.: Airborne Gamma-ray Spectrometry. Statistical Analysis of Airborne Gamma-ray Spectra. Ph.D.-thesis, October 1997, Department of Automation, Technical University of Denmark.

9. Bargholz, K.; Hovgaard, J. and Korsbech, U.: Standard methods for processing data from the Danish AGS system. Report IT-NT-36, IAU/DTU April 1998.

10. Danish Emergency Management Agency: NuCSpec ver. 2.1, 2000.

Bibliographic Data Sheet **NKS-55**

Title	Measurements of plume geometry and argon-41 radiation field at the BR1 reactor in Mol, Belgium.
Author(s)	Martin Drews[1)], Helle Karina Aage[2)], Kim Bargholz[3)], Hans Jørgensen[1)], Uffe Korsbech[2)], Bent Lauritzen[1)], Torben Mikkelsen[1)], Carlos Rojas-Palma[4)] and Raf Van Ammel[4)]
Affiliation(s)	[1)] Risø National Laboratory, Denmark [2)] Technical University of Denmark [3)] Danish Emergency Management Agency [4)] Belgian Nuclear Research Center (SCK•CEN), Belgium
ISBN	87-7893-109-6
Date	February 2002
Project	NKS/BOK-1.3
No. of pages	42
No. of tables	10
No. of illustrations	43
No. of references	10
Abstract	An atmospheric dispersion experiment was conducted using a visible tracer along with the routine releases of ^{41}Ar from the BR1 air-cooled research reactor in Mol. In the experiment, simultaneous measurements of the radiation field from the ^{41}Ar decay, the meteorology, the ^{41}Ar source term and plume geometry were performed. The visible tracer was injected into the reactor emission stack, and the plume cross section determined by Lidar scanning of the released aerosols. The data collected in the exercise provide a valuable resource for atmospheric dispersion and dose rate modeling.
Key words	Aerosols; Argon 41; BR-1 Reactor; Gamma Detection; Optical Radar; Plumes; Tracer Techniques.

Available from the NKS Secretariat, P.O. Box 30, DK-4000 Roskilde, Denmark.
Phone (+45) 46774045, fax (+45) 46774046, mail nks@catscience.dk, www.nks.org.